REPORT DOCUMENTATION PAGE

Form Approved
OMB No. 074-0188

1. AGENCY USE ONLY (Leave blank)	2. REPORT DATE	3. REPORT TYPE AND DATES COVERED
	Jan 1994	Revised technical report, 1994

4. TITLE AND SUBTITLE
Four Years of Global Cirrus Cloud Statistics Using HIRS

5. FUNDING NUMBERS
N/A

6. AUTHOR(S)
Donald P. Wylie, W. Paul Menzel, Harold M. Woolf, and Kathleen I. Strabala

7. PERFORMING ORGANIZATION NAME(S) AND ADDRESS(ES)
Space Science and Engineering Center
University of Wisconsin-Madison

Satellite Applications Laboratory
NOAA/NESDIS
Madison, Wisconsin 53706

8. PERFORMING ORGANIZATION REPORT NUMBER
N/A

9. SPONSORING / MONITORING AGENCY NAME(S) AND ADDRESS(ES)
SERDP
901 North Stuart St. Suite 303
Arlington, VA 22203

10. SPONSORING / MONITORING AGENCY REPORT NUMBER
N/A

11. SUPPLEMENTARY NOTES
Submitted July 1993, and revised January 1994.

12a. DISTRIBUTION / AVAILABILITY STATEMENT
Approved for public release: distribution is unlimited

12b. DISTRIBUTION CODE
A

13. ABSTRACT ***(Maximum 200 Words)***

Trends in global upper tropospheric transmissive cirrus cloud cover are beginning to emerge from a four year cloud climatology using NOAA polar orbiting HIRS multispectral infrared data. Cloud occurrence, height, and effective emissivity are determined with the CO_2 slicing technique on the four years of data (June 1989-May 1993). There is a global preponderance of transmissive high clouds, 42 % on the average; about three fourths of these are above 500 hPa and presumed to be cirrus. In the ITCZ a high frequency of cirrus (grater than 50%) is found at all times; a modest seasonal movement tracks the sun. Large seasonal changes in cloud cover occur over the oceans in the storm belts at mid-latitudes; the concentrations of these clouds migrate north and south with the seasons following the progressions of the subtropical highs (anticyclones). More cirrus is found in the summer than in the winter in each hemisphere.

This paper reports on the investigation of seasonal changes with multispectral observations from polar orbiting HIRS (High resolution Infrared Radiation Sounder).

14. SUBJECT TERMS
NOAA polar orbiting HIRS multispectral infrared data, anticyclones, SERDP, AVHRR

15. NUMBER OF PAGES
57

16. PRICE CODE
N/A

17. SECURITY CLASSIFICATION OF REPORT	18. SECURITY CLASSIFICATION OF THIS PAGE	19. SECURITY CLASSIFICATION OF ABSTRACT	20. LIMITATION OF ABSTRACT
unclass	unclass	unclass	UL

NSN 7540-01-280-5500

Standard Form 298 (Rev. 2-89)
Prescribed by ANSI Std. Z39-18
298-102

Appendix A

FOUR YEARS OF GLOBAL CIRRUS CLOUD STATISTICS USING HIRS

Donald P. Wylie

Space Science and Engineering Center

University of Wisconsin-Madison

W. Paul Menzel and Harold M. Woolf

Satellite Applications Laboratory

NOAA/NESDIS

Madison, Wisconsin 53706

Kathleen I. Strabala

Space Science and Engineering Center

University of Wisconsin-Madison

submitted July 1993

revised January 1994

Abstract

Trends in global upper tropospheric transmissive cirrus cloud cover are beginning to emerge from a four year cloud climatology using NOAA polar orbiting HIRS multispectral infrared data. Cloud occurrence, height, and effective emissivity are determined with the CO_2 slicing technique on the four years of data (June 1989 - May 1993). There is a global preponderance of transmissive high clouds, 42% on the average; about three fourths of these are above 500 hPa and presumed to be cirrus. In the ITCZ a high frequency of cirrus (greater than 50%) is found at all times; a modest seasonal movement tracks the sun. Large seasonal changes in cloud cover occur over the oceans in the storm belts at mid-latitudes; the concentrations of these clouds migrate north and south with the seasons following the progressions of the subtropical highs (anticyclones). More cirrus is found in the summer than in the winter in each hemisphere.

A significant change in cirrus cloud cover occurs in 1991, the third year of the study. Cirrus observations increase from 35% to 43% of the data, a change of 8 percentage points. Other cloud forms, opaque to terrestrial radiation, decrease by nearly the same amount. Most of the increase is thinner cirrus with infrared optical depths below 0.7. The increase in cirrus happens at the same time as the 1991-92 El Nino/Southern Oscillation (ENSO) and the eruption of Mt. Pinatubo. The cirrus changes occur at the start of the ENSO and persist into 1993 in contrast to other climatic indicators which return to near pre-ENSO and volcanic levels in 1993.

1. Introduction

Cirrus clouds are crucially important to global radiative processes and the thermal balance of the Earth; they allow solar heating while reducing infrared radiation cooling to space. Models of climate changes must simulate these clouds correctly to account for radiometric effects properly in the Earth's energy budget. Past estimates of the variation of cloud cover and the Earth's outgoing longwave radiation have been derived primarily from longwave infrared window (10-12 microns) radiances observed from polar orbiting and geostationary satellites (Rossow and Lacis, 1990; Gruber and Chen, 1988; Stowe et al., 1988). The occurrence of transmissive clouds has been under-estimated in these single band approaches. Recently, multispectral techniques have been used to better detect cirrus in global (Wu and Susskind, 1990) and North American (Wylie and Menzel, 1989; Menzel et al., 1992) cloud studies.

This paper reports on the investigation of seasonal changes in semi-transparent or cirrus global cloud cover with multispectral observations from polar orbiting HIRS (High resolution Infrared Radiation Sounder). Clouds partially transparent to terrestrial radiation are separated from opaque clouds in four year statistics of cloud cover (Wylie and Menzel, 1989). Transmissive or cirrus clouds are found in roughly 40% of all satellite observations.

The HIRS observations in the carbon dioxide absorption band at 15 microns are used to calculate these cloud statistics. The CO_2 slicing algorithm calculates both cloud top pressure and effective emissivity from radiative transfer principles. Various CO_2 algorithms have been described in the literature (Chahine, 1974; Smith et al., 1974; McCleese and Wilson, 1976; Smith and Platt, 1978; Wielicki and Coakley, 1981; Menzel et al., 1983) and applications to data from the geostationary sounder VAS (VISSR Atmospheric

Sounder) and the polar orbiting sounder HIRS have been published (Wylie and Menzel, 1989; Menzel et al., 1986; Susskind et al., 1987; Menzel et al., 1989; Eyre and Menzel, 1989).

2. Technique

Cirrus clouds often appear warmer in the infrared window band than the ambient air temperature at their altitude because they are transmitting radiation from below. This occurs in more than 40% of the satellite data, of which roughly half is often misinterpreted as lower non-cirrus clouds. The CO_2 slicing technique is capable of correctly identifying most of these clouds. Using the HIRS infrared bands with partial CO_2 absorption, cloud top pressure and effective emissivity are calculated for each observational area. CO_2 slicing does not estimate cloud base pressure. Partially transmissive clouds are distinguished during daylight and night over water and land. The description of the technique and details of its application with HIRS data are presented in Menzel et al. (1986 and 1989) and are repeated in Appendix A of this paper; there are similarities to the application with VAS data described in Wylie and Menzel (1989).

Effective emissivity refers to the product of the fractional cloud cover, N, and the cloud emissivity, ϵ, for each observational area (roughly 20 km by 20 km). When $N\epsilon$ is less than unity, HIRS may be observing broken cloud ($N < 1$, $\epsilon = 1$), overcast transmissive cloud ($N = 1$, $\epsilon < 1$), or broken transmissive cloud ($N < 1$, $\epsilon < 1$). All of these possibilities imply an observation where the HIRS radiometer detects radiation from below a cloud layer as well as radiation from the cloud layer top. All observations where the effective emissivity is less than 0.95 are labelled as "cirrus" in this

paper. Effective emissivity observations greater than 0.95 are considered to be opaque clouds.

Cirrus usually are transmissive and exhibit spatial variations at scales ranging from hundreds of kilometers to smaller than the field of view (FOV) of the instrument. The assumption is that more of the semi-transparency for a given field of view is due to cloud emissivity being less than one than due to the cloud not completely covering the field of view. Comparison of Advanced Very High Resolution Radiometer (AVHRR) one kilometer resolution cloud data and HIRS 20 kilometer resolution cloud effective emissivity determinations supports this. For effective emissivity determinations greater than 0.50, almost all of the variation from one FOV to another is caused by changes in emissivity and not cloud fraction. For effective emissivities less than 0.50, most of the variation is still being caused by changes in cloud emissivity fraction but some is now being caused by changes in cloud fraction. Appendix B presents this comparison. Thus for most synoptic regimes, especially in the tropics and subtropics, this assumption appears reasonable and it is supported in the literature (Wielicki and Parker, 1992; Baum et al., 1992).

In multiple cloud layers, the technique is limited to finding the height of only the highest cloud layer. Multiple layers often can be inferred from inspection of neighboring pixels where holes in the upper layer occur. Comparison to cloud reports from ground observers indicate that 50% of the time when the CO_2 technique detects an upper tropospheric cloud, one or more lower cloud layers also is present (Menzel and Strabala, 1989). When an opaque cloud underlies a transmissive cloud, the height of the transmissive cloud is estimated to be too low by as much as 100 hPa (Menzel et al., 1992). The largest error occurs when the underlying opaque layer is in the middle troposphere (400-700 hPa) and the upper cirrus layer is very thin. The error

is small when the opaque cloud is near the surface or close to the upper transmissive layer. The error in effective emissivity of the transmissive cloud increases as the opaque layer approaches the transmissive layer; when they are coincident the effective emissivity is set to one.

The processing procedure is briefly outlined here. More details are given in Appendix A. CO_2 slicing cloud top pressures are calculated when the cloud forcing (clear minus cloudy radiance is greater than five times the instrument noise level); otherwise the infrared window temperature is used to determine an opaque cloud top pressure. Fields of view are determined to be clear if the moisture corrected 11.1 micron brightness temperature is within 2.5 C of the known surface temperature (over land this is inferred from the NMC Medium Range Forecast (MRF) model analysis; over the oceans this is the NOAA NESDIS sea surface temperature analysis).

In this four year study, HIRS data from NOAA 10, 11, and 12 are sampled to include only data from every third FOV on every third line with zenith angle less than 10 degrees. With two satellites, about one half of the Earth is sampled each day. Morning orbits over land are rejected from the data because a good guess of the morning land surface temperature is unavailable and therefore discerning cloudy from clear FOVs is difficult. In the Arctic and Antarctic, the HIRS bands are inspected for the presence of surface temperature inversions which are assumed to be indicators of clear sky.

3. Global Cloud Statistics

A statistical summary of over 15 million cloud observations from HIRS between June 1989 through May 1993 is shown in Table 1. High clouds above 400 hPa comprise 24% of the observations. 27% of the observations are of clouds between 400 hPa and 700 hPa. Low clouds below 700 hPa are found 26% of the

time. Cloud free conditions are found 23% of the time. Cirrus and transmissive clouds (with effective emissivities less than 0.95) are found in 42% of our observations; they range from 100 to 800 hPa. The 12% transmissive observations below 500 hPa are most likely broken clouds. Clouds opaque to infrared radiation (with effective emissivities greater than 0.95) are found 35% of the time. The global average cloud effective emissivity (global average of $N\epsilon$) is found to be 0.54; Warren et al. (1988) report a global cloud fraction of 0.61 from ground observations.

The frequency of different cloud observations is used to indicate the probability that a given HIRS field of view is found to contain a certain type of cloud. The frequency of all clouds over land is 67% versus 79% over ocean; the frequency of cirrus clouds over land is 39% versus 43% over ocean. High clouds above 500 hPa prefer land over ocean (37% versus 34%). Thin clouds ($N\epsilon \leq 0.50$ or infrared optical depth $\tau < 0.7$) prefer ocean over land (22% versus 18%).

As the satellite views from above the atmosphere, high clouds are found in preference to low clouds. Broken low cloud fields are reported as opaque low clouds because the CO_2 slicing technique is unable to estimate the cloud fraction below the sensitivity peaks in the CO_2 bands. Transmissive clouds cover the range of effective emissivities from 0.0 to 0.95 fairly uniformly.

The CO_2 slicing technique is subject to some errors that have been discussed in Menzel et al. (1992). The large observation area (20 km by 20 km) produces results where transmissive cloud observations are over-estimated; cloud edges and clear sky within a FOV are incorrectly estimated to be transmissive cloud in roughly 5% of the FOVs. Conversely, the HIRS lack of sensitivity to very thin clouds in roughly 5% of the FOVs causes transmissive clouds to be incorrectly classified as lower opaque clouds (Wylie and Menzel,

1989). And finally, the top down view of the satellite reveals high clouds in preference to lower occluded clouds. These errors are largely offsetting. Overall, the frequency of clear sky observations in Table 1 is believed to be valid within 3%.

A similar multispectral analysis of transmissive clouds was previously published for continental United States using GOES/VAS data (Wylie and Menzel, 1989; Menzel et al., 1992). A comparison of the CO_2 slicing analysis of coincident data from both the GOES/VAS and NOAA/HIRS is shown in Appendix C. The two analyses find similar frequency of clear sky. However, the HIRS data produce more transmissive cloud observations than the VAS. We suspect that these differences appear because the radiance noise of the HIRS is less than that of the VAS and hence HIRS cloud parameters for thin clouds will be determined more often from CO_2 slicing and less often from the infrared window. When observed and clear FOV radiance observations differ by less than five times the noise in the radiometric measurements, low opaque clouds are inferred. The smaller radiometric noise of the HIRS allows it to produce CO_2 slicing solutions for thin clouds more consistently. In addition the larger HIRS FOV reduces the ability of the HIRS to find breaks or holes in the upper level cloud fields. The VAS with a smaller FOV is able to report more of these holes whereas the HIRS averages them in with the cloud field. These two differences would cause the HIRS to indicate more transmissive cloud than the VAS.

Comparison with the results of the International Satellite Cloud Climatology Project (ISCCP) reveal that this HIRS multispectral analysis is finding roughly twice as mnay transmissive clouds than the ISCCP visible and infrared window analysis. Jin and Rossow (1994) studied collocated ISCCP and HIRS results for four months (July 1989, October 1989, January 1990, and April

1990); HIRS finds 76% cloud cover (80% over water and 65% over land) while ISSCP finds 63% cloud cover (68% over water and 51% over land). Most of this difference is attributed to HIRS detection of optically thin clouds (infrared optical depth less than 0.7); HIRS finds 17% while ISSCP finds only 7%. However HIRS finds about 3% less low opaque cloud than ISSCP (22% versus 25% respectively). Hartmann et al. (1992) present one year (March 1985 -February 1986) of ISSCP data and find semi-transparent cloud (visible optical depth less than 9.4 which corresponds roughly to infrared optical depth less than 4.7) 21% of the time; HIRS finds 42% in the four years of this study (June 1989 - May 1993). HIRS finds twice as much semi-transparent cloud than ISCCP high in the atmosphere (21% to 10% respectively) and at mid-levels (21% to 11% respectively). HIRS finds less opaque cloud at high and middle levels above 700 hPa than ISSCP (10% to 15% respectively), but the low cloud detection is comparable (25% to 26% respectively). HIRS finds less clear sky in the four years than the one year of ISSCP that Hartmann et al. (1992) studied (23% to 36% respectively). Both of these comparisons point to the ISSCP difficulty in detecting thin transmissive clouds; if one were to exclude clouds with infrared optical depths less than 0.7 from the HIRS data (roughly 20% of the observations) and increase the frequency of low opaque clouds in the HIRS data (adding roughly 5%), all adjusted HIRS cloud categories would agree with Jin and Rossow (1994) and Hartmann et al. (1992) to within a few percent.

4. Seasonal and Geographical Trends

Table 2 presents the seasonal variation of clouds by classifications of clear sky, thin clouds ($N\epsilon < 0.5$), thick clouds ($0.5 < N\epsilon < 0.95$), and opaque clouds ($N\epsilon > 0.95$) and by height categories of high (cloud pressure less than 400 hPa), middle (cloud pressure between 400 and 700 hPa), and low (cloud

pressure greater than 700 hPa). The all season four year summary is also included for comparison. Little variation is found in the global boreal summer versus winter cloud statistics. A few percent more cirrus and less clear sky are found in the boreal winter. Hartmann et al. (1992) report similar seasonal statistical differences.

Figure 1 shows the geographical distribution of cirrus clouds in the summer and winter seasons (darker regions indicate more frequent cloud occurrence). The months of December, January, and February were summarized for the boreal winter (austral summer) and the months of June, July, and August were used for the boreal summer (austral winter). The seasonal summaries were compiled using a uniformly spaced grid of 2 degree latitude by 3 degree longitude. Each grid box for each season has at least 500 observations.

The major features of the four year summary have not changed appreciably from those reported in the two year summary (Wylie and Menzel, 1991). The Inter-Tropical Convergence Zone (ITCZ) is readily discernible as the region of more frequent cirrus (darker band in the tropics); the mid-latitude storm belts are also evident. The ITCZ is seen to move north with the sun. This seasonal migration is also apparent in the latitudinal summaries shown in Figure 2. The subtropical high pressure systems are seen in the region of less frequent cirrus cover (white band in the subtropics). Over the Indonesian region the ITCZ expands in latitudinal coverage from boreal winter to summer. In the central Pacific Ocean, the ITCZ shows both a southern and northern extension during the boreal winter months.

In the southern hemisphere, the eastern Pacific Ocean off South America and the eastern Atlantic Ocean off Africa remain relatively free of cirrus clouds throughout the year. The southern hemispheric storm belt is evident

throughout the year. In the northern hemisphere mid-latitude storm belts, the frequency of cirrus clouds increases during the winter with the strengthening of the Aleutian Low in the north Pacific Ocean and the Icelandic Low in the north Atlantic Ocean. The North American cirrus cloud cover shows little seasonal change, agreeing with a previous GOES/VAS analysis (Menzel et al., 1992). Large convective development occurs during the austral summer (boreal winter) in South America and Africa, which is readily apparent in the increased occurrence of high cirrus clouds.

A large seasonal change is found over Antarctica, where few clouds of any altitude are reported in the austral winter. The HIRS data do not show polar stratospheric clouds, which occur commonly over Antarctica in the months of June, July, and August. Polar stratospheric clouds apparently do not attenuate the HIRS bands sufficiently to mask out the strong inversions below them.

These seasonal changes in geographical distribution of global transmissive clouds are largely in agreement with the one year ISSCP results shown in Hartmann et al. (1992). The ITCZ expands in the Indonesian region in the boreal summer, the Icelandic low creates more cirrus in the boreal winter, convective development in South America and Africa is obvious in the austral summer, and the eastern Atlantic and Pacific Oceans in the southern hemisphere stay mostly free of cirrus clouds year round. As discussed previously, the ISSCP data indicate about half the transmissive clouds that the HIRS data does.

Upper tropospheric clouds (above 500 hPa) are discussed in the following paragraphs. Figure 2 shows the zonal distribution of high clouds, which includes both the transmissive and opaque clouds (30% and 5% of all observations respectively). The frequent occurrence of high clouds in the

ITCZ is prominent as the central maximum; the mid-latitude storm belts are evident in the secondary maxima. Seasonal shifts in the ITCZ are apparent over both land and ocean, as the ITCZ moves north and south with the sun. The frequency of high clouds over land increases strongly from the equator to 30 S during the austral summer. The main contributors are the Amazon Basin of South America and the Congo of Africa. The high clouds over the southern hemispheric storm belt, primarily over the oceans from 30 S to 70 S, remain constant throughout the year. The northern hemispheric land masses from 45 N to 65 N also show little seasonal change in high cloud cover. Jin and Rossow (1994) indicate that the HIRS zonal distribution of high cloud is in very good agreement with the ISSCP data, when clouds with infrared optical depth less than 0.7 are omitted from the HIRS data.

Light cirrus show smaller seasonal changes. The latitudinal distribution of thin transmissive ($N\epsilon < 0.5$ or infrared optical depth $\tau < 0.7$) clouds over ocean and over land is shown in Figure 3. The occurrence is somewhat more likely over ocean; this disagrees with Warren et al. (1988) who found more cirrus over land than ocean in their ground based observations. A modest peak from 10 S to 10 N is evident both over land and ocean. Thin transmissive clouds appear globally with a frequency of 5 to 40%.

5. Trends in the Four Years

The progression of cloud cover from year 1 (June 1989 - May 1990) to year 2 (June 1990 - May 1991), from year 2 to year 3 (June 1991 - May 1992), and from year 3 to year 4 (June 1992 - May 1993), is shown in Table 3. Thin clouds refer to $N\epsilon < 0.5$ (infrared optical depth $\tau < 0.7$), thick refers to $0.5 < N\epsilon < 0.95$ ($0.7 < \tau < 3.0$). The change from year 1 to year 2 is imperceptible. The change from year 2 to year 3 is large and very obvious;

opaque clouds decrease by 7% and cirrus increases by 8%. Cirrus appears much more frequently in the year 3 data than in previous years; conversely opaque cloud appears much less frequently. The probability of clear sky remains stable. The change from year 3 to year 4 is small; cloud cover increases by approximately 3%.

The geographical distribution of the difference in the probability of cirrus occurring in the boreal summer of 1990 minus boreal summer 1989 is shown in Figure 4a (upper left panel). Differences greater than 12% are scattered about, with no discernible pattern. Coherent changes are apparent only in the Timor Sea off the northwest coast of Australia (where a decrease of cirrus occurs) and in the Pacific Ocean east of Papua New Guinea (where an increase of cirrus occurs). Figure 4b shows the corresponding difference for the boreal winters of 1990-91 minus 1989-90 (upper left panel). Again there is not very much difference. The only features are the increase of cirrus in the Coral and Timor Seas and the decrease of cirrus in the Indian Ocean west of Australia (representing a westward shift from Fig 4a).

A change in cirrus coverage in the summer of 1991 with respect to the summer of 1990 is obvious (Figure 4a upper right panel). Coherent increases of cirrus greater than 12% are apparent along the southern edge of the ITCZ, in the southern mid-latitudes, the Indian Ocean, and in eastern Africa. Decreasing cirrus is indicated in the higher latitudes of the southern hemisphere. The boreal winter 1991-92 shows an even stronger increase in cirrus with respect to the winter 1990-1991 (Figure 4b upper right panel). The largest increases are in the central Pacific Ocean, in the Indian Ocean, and the northern hemisphere mid-latitudes. The central Pacific Ocean is also the location of an El Nino event where sea surface temperature anomalies greater than 2.0 C were reported in January 1992.

The patterns of increasing cirrus in the boreal summer 1991 are consistent with the decrease in net radiation from ERBE for August 1991 observations compared to the August average for the previous five years, especially over the Amazon, the central Atlantic Ocean, the African Congo, off the east African coast, the southern Indian Ocean, and the central Pacific Ocean (Minnis et al., 1993). In this HIRS study, more thin cirrus was found after the eruption of Mt. Pinatubo at the expense of opaque cloud. This is consistent with the hypothesized indirect effect of aerosols, which would cause more high thin cirrus cloud to be produced and to be longer lasting (Sassen, 1992).

In the fourth summer of this study, a slight cirrus decrease (Figure 4a lower left panel) is found in the southerly latitudes (50 S to 75 S) and in the Atlantic Ocean off the east coast of Africa. Elsewhere there is no recognizable pattern. Finally, Figure 4b (lower left panel) shows the difference for the boreal winters 1992-93 minus 1991-92. Cirrus probability decreases noticeably in the central Pacific Ocean (the location of a dramatic increase in sea surface temperature the previous winter), in the Gulf of Mexico and Central America (in contrast to the increase in the previous year), and off the west coast of Australia in the Indian Ocean (again the location of a noticeable increase the previous year). This last winter appears to be compensating for the local increases in cirrus from the previous winter.

The cirrus increase in 1991 (year 2 to year 3) is in concert with two major global events that effected most climatic data. They are summarized in Halpert and Ropelewski (1993). The first major event started in April 1991, when an increase in eastern Pacific Ocean temperatures signaled the start of an El Nino/Southern Oscillation (ENSO) event. Subsequently by October 1991, Outgoing Longwave Radiation (OLR) measurements from satellites and 850 hPa

wind observations showed large anomalies from climatic means. By January 1992, sea surface temperature anomalies in the eastern equatorial Pacific Ocean were greater than 2.0 C (NOAA, 1992). The second major event came in June 1991 with the eruption of Mt. Pinatubo, which set new records for ash and aerosol in the stratosphere. Aerosol optical depth measurements by Stowe et al. (1992) showed a dramatic increase in the tropics in the following months. This aerosol later spread to higher latitudes by the end of the year.

Figure 5 shows the monthly changes in these HIRS high cloud data for the four years. A major increase in global high clouds (solid line in Figure 5) begins in April 1991 coincident with the change in eastern Pacific Ocean temperatures. The frequency of high cloud observations (above 500 hPa) increases from 32% in March 1991 to 37% in June 1991 to 39% in December 1991. The largest high cloud increases are in the tropics (20 S to 20 N). Tropical high cloud frequency increases from 34% in March 1991 to 40% in June 1991 (long dash in Figure 5), while tropical light cirrus ($N\epsilon < 0.5$ or $\tau < 0.7$) increases even more from 23% in March 1991 to 31% in June 1991 (short dash in Figure 5). Examination of the local region in the eastern Pacific Ocean (10 S to 10 N, 110 W to 170 W) reveals even more dramatic changes (dot dash in Figure 5). Light cirrus observations change from near 25% frequency during the winter to over 40% in the summer. Seasonal and monthly changes are evident. In the boreal winter (December 1991 to February 1992) frequencies of 55-60% are found, well in excess of the previous years.

Changes in the satellite system are not the cause of the increased detection of cirrus and high cloud. In June 1991, NOAA 12 replaced to NOAA 10 as the sunrise and sunset satellite. NOAA 11, the midday and midnight satellite, maintained continuous operation through this entire four year period. Examination of NOAA 11 data only reveals the same changes. Thus we

conclude that the change in satellites had no effect on the trends evident in this data. The increase in stratospheric aerosol also should not have affected the cloud observations. The CO_2 sounding bands are in the 13 to 15 micron region of the infrared spectrum, which is beyond the portion of the spectrum affected by these very small stratospheric particles (Ackerman and Strabala, 1994).

It is also significant that the increase in cirrus and high cloud observations continue into 1993 with reduction only in small areas. The other climatic indicators such as the eastern Pacific Ocean temperatures, OLR, and 850 wind anomalies revert back to near normal (average) levels by July 1992. The increased detection of cirrus in the HIRS data persists beyond 1992 into 1993. We don't have an explanation for this persistence, but suggest that forces that cause and maintain cirrus (as described in Menzel et al. (1992)) are subtle and could be present even after other climatic anomalies have subsided.

6. Diurnal Trends

Diurnal variations in cloud cover are examined using the four observations from the two NOAA satellites each day. NOAA 11 passes over a given location at approximately 0200 to 0300 a.m. and p.m. local time (midnight and midday) every day while NOAA 10 and 12 have an overpass from 0700 to 0800 a.m. and p.m. local time (sunrise and sunset). These observations are analyzed in four time blocks of 6 hours each. Differences in the frequency of cloud observations from the daily mean are presented in Figure 6. The diurnal anomalies are expressed as the difference of the frequency of observation of cloud from the mean frequency using all observations at all times. Diurnal variations in cloud cover are discussed

only over water. Over land, two of the four satellite passes are not analyzed each day because the NMC model analysis does not track the strong diurnal variations in surface temperatures, especially in many desert areas. Over the ocean, the diurnal surface temperature change is presumed to be insignificant and the same NOAA/NESDIS sea surface temperature analysis is used for each satellite pass in this cloud analysis.

A diurnal cycle in all cloud observations (Figure 6), both cirrus and lower altitude cloud forms, is found mainly outside of the ITCZ. Maxima occur in the midnight overpass. Geographical diurnal variations (not shown) are strongest in the southeastern Atlantic and Pacific Oceans. Some variations are present in the northeastern Pacific Ocean, near the coasts of California and Baja, and in the central Atlantic Ocean to the African coast. The cycle appears to be stronger during the summer and is dominated by lower cloud forms, mostly marine stratus.

High clouds (above 500 hPa) show little diurnal pattern (see Figure 7). The frequency of these clouds changes by ±3 percentage points during the day at all latitudes. The largest diurnal variation is found near the ITCZ from the Equator to 15 N in the boreal summer. Thin cirrus ($N\epsilon < 0.5$ or $\tau < 0.7$) exhibit even smaller diurnal variations with no obvious pattern.

7. Summary and Conclusions

There continues to be a global preponderance of transmissive clouds 42% on the average for the four years covered by June 1989 to May 1993. About three fourths of these are above 500 hPa and presumed to be cirrus. In the ITCZ a high frequency of cirrus (greater than 50%) is found at all times; a modest seasonal movement tracks the sun. Large seasonal changes in cloud cover occur over the oceans in the storm belts at mid-latitudes; the

concentrations of these clouds migrate north and south with the seasons following the progressions of the subtropical highs (anticyclones). More cirrus is found in the summer than in the winter in each hemisphere (largely due to the ITCZ).

Large changes in cirrus and high cloud cover are found beginning in the spring-summer 1991. These cloud frequency increases occur in concert with the 1991-1992 ENSO and the Mt. Pinatubo volcanic eruption. Associated changes include an increase in sea surface temperature starting April 1991, anomalies in Outgoing Longwave Radiation and 850 hPa winds around October 1991, and a dramatic increase in stratospheric aerosol after June 1991. The cirrus and high cloud increase starts before Mt. Pinatubo's eruption and persists beyond the summer of 1992, at which time the ENSO anomalies are mostly gone and statospheric aerosol measurements are near their pre-eruption levels. Decreases in cirrus are seen in local regions, but higher occurrence of cirrus in the global average remains. There is no obvious explanation, other than thin cirrus are statistically persistent and do not exhibit large seasonal changes outside of the tropics whereas other cloud forms do show large seasonal variations.

The increase in cirrus and high cloud is accompanied by a corresponding decrease in satellite observations of lower altitude opaque clouds; overall cloudiness changed very little during this period. Obviously, a satellite detects lower cloud forms less when higher clouds become more prevalent. However, the trend reported in this paper of more transmissive high cloud and less low opaque cloud is loosely supported by appreciable decreases in precipitation in many regions of the world (Halpert and Ropelewski, 1993) during the 1991-1992 ENSO and volcanic period.

A similar increase in cloud cover also was reported in the 1982-83 ENSO by Weare (1992) using the NIMBUS-7 infrared analysis of Stowe et al. (1988). An increase in both the amount of cloud (all altitudes) and the average cloud height was found. The height increase indicated more high cloud in late 1982 and most of 1983 during the height of the ENSO. This is a similar trend which this HIRS analysis finds for the 1991-92 ENSO. We have no explanation for these changes in global cloud cover. This is the topic of future studies.

Appendix A. Technique Description

The HIRS radiometer senses infrared radiation in eighteen spectral bands that lie between 3.9 and 15 microns at 20 to 35 km resolution (depending upon viewing angle) in addition to visible reflections at the same resolution. The four bands in the CO_2 absorption band at 15 microns are used to differentiate cloud altitudes and the longwave infrared window band identifies the effective emissivity of the cloud in the HIRS FOV.

The CO_2 slicing technique is derived from the calculation of radiative transfer in an atmosphere with a single cloud layer. For a single level cloud element in a FOV the radiance observed at the satellite, $R(\eta)$, in spectral band η can be written

$$R(\eta) = (1 - N\epsilon) \{ B(\eta,T(P_s))\ \tau(\eta,P_s) + \int_{P_s}^{P_c} [B(\eta,T(p))\ d\tau/dp]\ dp \} + N\epsilon\ B(\eta,T(P_c))\ \tau(\eta,P_c) + \int_{P_c}^{0} [B(\eta,T(p))\ d\tau/dp]\ dp \qquad (1)$$

where $\tau(\eta,P)$ is the transmittance through the atmosphere for band η, $N\epsilon$ is the effective emissivity of the cloud in the FOV, and $B(\eta,T(P))$ is the Planck function for band η and temperature T at pressure level P. P_s is the surface pressure while P_c is the cloud top pressure. The four terms in Equation (1)

are the radiation emitted from the surface, the contribution from the atmosphere below the cloud, the cloud contribution, and the contribution from the atmosphere above the cloud. For a clear FOV ($N\epsilon = 0$), the satellite measured radiance R_{clr} is

$$R_{clr}(\eta) = B(\eta,T(P_s))\ \tau(\eta,P_s) + \int_{P_s}^{0} [B(\eta,T(p))\ d\tau/dp]\ dp\ . \qquad (2)$$

Subtracting the clear FOV radiance $R_{clr}(\eta)$ from the cloudy FOV radiance $R(\eta)$ yields the following result.

$$R(\eta) - R_{clr}(\eta) = - N\epsilon\ B(\eta,T(P_s))\ \tau(\eta,P_s) - N\epsilon \int_{P_s}^{P_c} [B(\eta,T(p))\ d\tau/dp]\ dp$$

$$+ N\epsilon\ B(\eta,T(P_c))\ \tau(\eta,P_c)\ . \qquad (3)$$

This is the cloud signal in the satellite measured radiances for spectral band η; it is the radiance difference of the cloudy FOV from neighboring clear FOVs. A simplified equation, after integration by parts, is

$$R(\eta) - R_{clr}(\eta) = N\epsilon \int_{P_s}^{P_c} [\tau(\eta,p)\ dB(\eta,T(p))/dp]\ dp\ . \qquad (4)$$

Following the work of Smith and Platt (1978), the ratio of the cloud signal for two spectral bands of frequency η_1 and η_2 viewing the same FOV can be written as

$$\frac{R(\eta_1) - R_{clr}(\eta_1)}{R(\eta_2) - R_{clr}(\eta_2)} = \frac{N\epsilon_1 \int_{P_s}^{P_c} [\tau(\eta_1,p)\ dB(\eta_1,T(p))/dp]\ dp}{N\epsilon_2 \int_{P_s}^{P_c} [\tau(\eta_2,p)\ dB(\eta_2,T(p))/dp]\ dp}\ . \qquad (5)$$

If the frequencies are close enough together, then $N\epsilon_1$ approximates $N\epsilon_2$, and one has an expression by which the pressure of the cloud (P_c) within the FOV can be calculated without apriori knowledge of the emissivity.

The left side of Equation (5) is determined from the satellite observed radiances in a given FOV and the clear air radiances inferred from spatial analyses of satellite clear radiance observations. The right side of Equation (5) is calculated from a temperature profile T(p) and the profiles of atmospheric transmittance for the spectral bands $\tau(\eta,P)$ as a function of P_c, the cloud top pressure. The calculation uses global analyses of temperature and moisture fields from the National Meteorological Center (NMC) and is performed at 50 hPa intervals from 1000 hPa to 100 hPa. For a given spectral band pair, the solution for P_c is the best match of observed and calculated ratios.

Once a cloud height has been determined, an effective emissivity (also referred to as effective cloud amount in this paper) is evaluated from the infrared window band data using the relation

$$N\epsilon = \frac{R(w) - R_{clr}(w)}{B[w, T(P_c)] - R_{clr}(w)} . \qquad (6)$$

Here $N\epsilon$ is the effective cloud amount observed in the window band, w represents the window band frequency, and $B[w, T(P_c)]$ is the opaque cloud radiance in the window band.

Using the ratios of radiances of the four CO_2 spectral bands, four separate cloud top pressures can be determined (14.2/14.0, 14.0/13.7, 14.0/13.3, and 13.7/13.3). Whenever $(R-R_{clr})$ is within five times the noise response of the instrument (conservatively estimated at roughly 1 mW/m2/ster/cm-1), the resulting P_c is rejected. Using the measured infrared window radiance and the four cloud top pressures, four calculations of effective emissivity are also made. As described by Menzel et al. (1983), the most representative cloud height and effective emissivity are those that best satisfy the radiative transfer equation for the four CO_2 spectral bands.

If no ratio of radiances can be reliably calculated because ($R-R_{clr}$) is within five times the instrument noise level, then a cloud top pressure is calculated directly from the comparison of the HIRS observed 11.1 micron infrared window band brightness temperature with an in situ temperature profile and the effective emissivity is assumed to be unity. In this way, all clouds are assigned a cloud top pressure either by CO_2 or infrared window calculations.

Fields of view are determined to be clear or cloudy through inspection of the 11.1 micron brightness temperature with an 8.3 or 12.0 micron band correction for moisture absorption. The band differences (11.1 - 8.3 micron for NOAA 10 and 12, or 11.1 - 12.0 micron for NOAA 11) were used to lower the threshold for clear-cloudy decisions in areas were water vapor affected the window band. This threshold change varied from 0 C near the poles in dry air masses to as high as 7 C in the moist tropical atmospheres. If the moisture corrected 11.1 micron brightness temperature is within 2.5 C of the known surface temperature (over land this is inferred from the NMC Medium Range Forecast (MRF) model analysis; over the oceans this is the NOAA/NESDIS sea surface temperature analysis), then the FOV is assumed to be clear (P_c = 1000 hPa) and no cloud parameters are calculated.

The HIRS data are calibrated and navigated by NOAA/NESDIS. These data are transmitted daily to the Man computer Interactive Data Access System (McIDAS) at the University of Wisconsin-Madison. The HIRS data from NOAA 10, 11, and 12 are sampled to make the processing more manageable. Every third pixel on every third line is used. The data are also edited for zenith angle, eliminating data over 10^o to assure top down viewing of the clouds and to minimize any problems caused by the increased path length through the atmosphere of radiation upwelling to the satellite. The resulting coverage is

restricted to approximately the center one third of the orbit swath. With two satellites, about one half of the Earth is sampled each day.

Morning orbits over land are not used because the surface temperature analysis over subtropical deserts is often warmer than the HIRS data; this causes cloud free areas to be mistaken as clouds. However, morning orbits over the oceans are used because no diurnal temperature change of the surface is assumed.

In the Arctic and Antarctic, the HIRS bands are inspected for the presence of surface temperature inversions. Over high altitude areas of Antarctica and Greenland, the HIRS 700 hPa band is often warmer than the window band. We assume that this indicates the presence of surface inversions from radiative cooling under clear skies. Surface inversions normally cannot be seen by the HIRS, but over polar high altitude continents the thermal contrast between 700 hPa and the elevated surface is often large enough to be detected. When the 700 hPa band is warmer than the window band, the observation is classified as cloud free. When the 700 hPa band is within 2.0 C of the window band, we assume that both bands saw the top of a cloud and the observation is classified as cloudy.

Appendix B. Comparison of AVHRR and HIRS cloud fractions.

In classifying transmissive cloud observations where the HIRS radiometer detects radiation from below a cloud layer as well as radiation from the cloud layer itself, we assume that more of the semi-transparency for a given field of view is due to cloud emissivity being less than one than due to the cloud not completely covering the HIRS 20 km field of view. In order to investigate this assumption more thoroughly, the effective emissivities $N\epsilon_H$ from the HIRS

CO_2 slicing are compared to cloud fractions N_A inferred from 1 km Advanced Very High Resolution Radiometer (AVHRR) data.

Figure 8 shows the plot of AVHRR cloud fraction N_A (determined from the number of AVHRR FOVs where the moisture corrected infrared window brightness temperatures is 2 C colder than NOAA/NESDIS sea surface temperature analysis within a collocated HIRS FOV) versus the HIRS CO_2 slicing effective emissivity $N\epsilon_H$. Roughly 100 comparisons are made for data from 6 and 12 January 1994 covering 20 N to 40 N in the western Atlantic Ocean (Figure 9 shows the AVHRR infrared window image for 6 January 1994). FOVs with clouds tops below 700 hPa are not included in the comparison because the CO_2 slicing algorithm is not used below that altitude. These data include subtropical clouds, high clouds from a cold front, and post cold frontal clouds.

Three-fourths of the HIRS CO_2 cloud observations are found to be completely cloud covered in the AVHRR data (N_A between 0.90 and 1.00.). This is in good agreement with the work of Baum et al. (1992), where 60% of the HIRS FOVs were found to be completely cloud covered in the AVHRR data. The remaining fourth of the HIRS cloudy FOVs, where N_A is less than 0.90, have $N\epsilon_H$ less than 0.45. It appears that for thick cloud ($N\epsilon_H > 0.50$) the FOV is always completely cloud covered ($N_A = 1.0$); for thin cloud ($N\epsilon_H < 0.50$) the FOV is almost always more than half covered with cloud ($0.50 < N_A < 1.0$). Wielicki and Parker (1992) also found that cirrus clouds have considerable spatial coherence and that most of the effect of sensor resolution is very weak on cirrus cloud cover estimates.

Figure 8 confirms the assertion that cloud emissivity and not cloud fraction is the dominant parameter in FOVs observed to have transmissive clouds. If cloud fraction, N, dominates and emissivity, ϵ, of the cloud is not significant in the CO_2 slicing determination, then all points would lie on

the $N_A = N\epsilon_H$ line. If ϵ variation from FOV to FOV dominates N variation, then the points would lie on or close to the $N_A = 1.0$ ordinate line. Clearly for $0.5 < N\epsilon_H < 1.0$, the cloud emissivity is the dominate cause of semi-transparency. Cloud fraction causes little change in observed radiance from one FOV to another. For $0.0 < N\epsilon_H < 0.5$, the cloud emissivity is the major cause, but cloud fraction is responsible for some of the variation.

Appendix C. Comparison of the NOAA/HIRS and the GOES/VAS cloud analyses.

The CO_2 slicing technique has been used to process cloud parameters with GOES/VAS data for four years prior to the start of the NOAA/HIRS analysis reported here (see Wylie and Menzel, 1989, and Menzel et al., 1992). The GOES/VAS algorithm uses the same equations as shown in Appendix A. However, there are differences in the data and methods used in handling of the data. (1) The GOES/VAS has three bands in the CO_2 absorption region of the spectrum whereas the HIRS has four bands; the VAS does not have the 13.7 micron band which has additional mid-level sensitivity. (2) The GOES/VAS FOV (10 X 10 km) is smaller than the HIRS FOV (20 X 20 km); the VAS algorithm averages three FOVs for each cloud determination representing a 300 km^2 observation area and a sample noise of roughly 0.8 mW/m2/ster/cm-1, while the HIRS algorithm uses a single FOV representing a 400 km^2 observation area with sample noise roughly 0.2 mW/m2/ster/cm-1. (3) Surface topographic heights are used in the HIRS algorithm, while they are not in the VAS algorithm; the surface pressure in Equation (5) of Appendix A is determined from topography for the HIRS solutions while all VAS solutions assume a surface of 1000 hPa. This affects the VAS results over the Rocky Mountains by 50 hPa or less. (4) A separate sea surface temperature analysis is used in the HIRS processing while the VAS processing uses the same MRF model surface temperature analysis both over land

and water. The VAS land surface temperatures are corrected using the SVCA hourly reports, whereas the HIRS are not. This will affect the determination of low cloud with the window band, but it will have almost no effect on CO_2 algorithm solutions since only one of the bands sees the ground.

Single FOV comparisons of HIRS and VAS cloud parameter determinations are attempted. For several days during the 1986 FIRE (First International Satellite Cloud Climatology Project Experiment) in transmissive cloud conditions, over 100 collocated single FOV observations within 15 minutes were accomplished. CO_2 slicing cloud heights determined by the HIRS are 20 hPa larger (lower altitude) on the average than those from the VAS in the single FOV comparison; effective emissivities average 0.05 higher on the VAS than the HIRS. Fluctuations are on the order of 100 hPa for cloud top pressure and 0.30 for effective emissivity. In this single FOV study, the VAS and HIRS cloud parameters compare within the estimated errors (Menzel et al., 1992). However, these results, while reassuring, must be viewed with some caution. Collocation over the same cloud element is very difficult as the satellite sensors have different FOVs, viewing times, and viewing angles.

A more meaningful comparison of HIRS and VAS cloud analyses is the seasonal average of the frequencies of cloud observations over North America for the four years of the HIRS study (June 1989 to May 1993). Table 4 shows the summary of the four winter seasons (December, January, February) and four summer seasons (June, July, August) of the HIRS cloud observations covering the North American region (29 N to 49 N and 70 W to 130 W) as well as the corresponding seasonal summary of the VAS over the same area and time period. Both HIRS and VAS find roughly the same amount of seasonal cloud cover (70% HIRS and 73% VAS in the summer and 76% HIRS and 78% VAS in the winter). However, HIRS reports more tranmissive cirrus in both winter and summer, 45%

HIRS to 33% VAS in winter and 35% HIRS to 27% VAS in summer. In particular, HIRS has 10 to 15% more mid-level (400 to 700 hPa) transmissive observations than the VAS. On the other hand VAS has 10% more low level opaque cloud observations. This is caused primarily by the larger noise in the VAS sensor which inhibits CO_2 slicing solutions for smaller cloudy versus clear radiance contrasts and identifies the cloud as low opaque in the infrared window solution.

The geographical distribution of the probabilities of high clouds above 500 hPa in each season computed from VAS and HIRS are presented in Figure 10. The cloud cover patterns are similar. In the winter, both the HIRS and VAS show higher probability of cloud cover over the Pacific northwest, the Rocky Mountains, and along the Gulf of Mexico and the eastern shore (40 to 60%), while they indicate a lower probability (20 to 40%) in the southwest over Baja Mexico. There is some disagreement in the northeast where VAS sees 20% more clouds than HIRS; this may be attributed to the large viewing angle of the VAS. In the summer, the cloud cover reduces (down by 20%) along the west coast and in the southern states, but it persists in the Rocky Mountains and along the eastern shore in both HIRS and VAS. Again there is disagreement in the northeast, where HIRS now sees 20% more cloud. Some of the moderate disagreement in both seasons over the oceans can be attributed to the difference in the sea surface temperature analysis used for HIRS versus VAS (as mentioned above).

In summary, the HIRS finds more mid-level (400-700 hPa) transmissive clouds and fewer low level opaque clouds than the VAS, but agrees with it in overall cloud reports. The geographical distribution of cloud reports from HIRS is similar to that from VAS, especially when a small VAS view angle is maintained.

Acknowledgments

This work was supported by Grants N00014-85-K-0581 and N00014-87-K-0436 of the Office of Naval Research and Grant NAG1-553 and Contract NAS5-31367 from the National Aeronautics and Space Administration and Grant ATM-8703966 from the National Science Foundation and Contract 50-WCNE-8-06058 from the National Oceanic and Atmospheric Administration and Grant F19628-91-K-0007 from the United States Air Force Geophysics Laboratory.

References

Ackerman, S. A. and K. I. Strabala, 1994: Satellite remote sensing of H2SO4 aerosol using the 8-12 micron window region: application to Mount Pinatubo. submitted to *J. Appl. Meteor.*

Baum, B. A., B. A. Wielicki, and P. Minnis, 1992: Cloud-property retrieval using merged HIRS and AVHRR data. *J. Appl. Meteor.*, **31**, 351-369.

Chahine, M. T., 1974: Remote sounding of cloudy atmospheres. I. The single cloud layer. *J. Atmos. Sci.*, **31**, 233-243.

Eyre, J. R., and W. P. Menzel, 1989: Retrieval of cloud parameters from satellite sounder data: A simulation study. *J. Appl. Meteor.*, **28**, 267-275.

Gruber, A., and T. S. Chen, 1988: Diurnal variation of outgoing longwave radiation. *J. Clim. Appl. Meteor.*, **8**, 1-16.

Hartmann, D. L., M. E. Ockert-Bell, and M. L. Michelsen, 1992: The effect of cloud type on the Earth's energy balance: global analysis. *J. Climate*, **5**, 1281-1304.

Halpert, M. S. and C. F. Ropelewski, 1993: Fourth Annual Climate Assessment, 1992. U. S. Dept of Commerce NOAA-NWS Climate Analysis Center, 90 pp.

Jin, Y. and W. B. Rossow, 1994: Investigation and Comparison of ISCCP and HIRS high level clouds. Eighth Conference on Atmospheric Radiation held 22-28 January 1994 in Nashville, TN, AMS publication, 64-65.

McCleese, D. J. and L. S. Wilson, 1976: Cloud top height from temperature sounding instruments. *Quart. J. R. Met. Soc.*, 102, 781-790.

Menzel, W. P., W. L. Smith, and T. R. Stewart, 1983: Improved cloud motion wind vector and altitude assignment using VAS. *J. Clim. Appl. Meteor.*, 22, 377-384.

Menzel, W. P., D. P. Wylie, and A. H.-L. Huang, 1986: Cloud top pressures and amounts using HIRS CO_2 channel radiances. Technical Proceedings of the Third International TOVS Study Conference, 13-19 August 1986, Madison, WI, 173-185.

Menzel, W. P. and K. I. Strabala, 1989: Preliminary report on the demonstration of the VAS CO_2 cloud parameters (cover, height, and amount) in support of the Automated Surface Observing System (ASOS). NOAA Tech Memo NESDIS 29.

Menzel, W. P., D. P. Wylie, and K. I. Strabala, 1989: Characteristics of global cloud cover derived from multispectral HIRS observations. Technical Proceedings of the Fifth International TOVS Study Conference, 24-28 July 1989, Toulouse, France, 276-290.

Menzel, W. P., D. P. Wylie, and K. I. Strabala, 1992: Seasonal and diurnal changes in cirrus clouds as seen in four years of observations with the VAS. *J. Appl. Meteor.*, 31, 370-385.

Minnis, P., E. F. Harrison, L. L. Stowe, G. G. Gibson, F. M. Denn, D. R. Doeling, and W. L. Smith, Jr., 1993: Radiative climate forcing by the Mount Pinatubo eruption. *Science*, 259, 1411-1415.

NOAA, Climate Analysis Center, 1992: Near real time analysis ocean/atmosphere for January 1992. Climate Diagnostics Bulletin No. 92/1, Kousky, V. E. (ed)

Rossow, W. B., and A. A. Lacis, 1990: Global and seasonal cloud variations from satellite radiance measurements. Part II: Cloud properties and radiative effects. *J. Climate*, **3**, 1204-1253.

Sassen, K., 1992: Evidence of liquid phase cirrus cloud formation from volcanic aerosols: Climatic implications. *Science*, **257**, 516-519.

Smith, W. L., H. M. Woolf, P. G. Abel, C. M. Hayden, M. Chalfant, and N. Grody, 1974: Nimbus 5 sounder data processing system. Part I: Measurement characteristics and data reduction procedures. NOAA Tech. Memo. NESS 57, 99pp.

Smith, W. L., and C. M. R. Platt, 1978: Intercomparison of radiosonde, ground based laser, and satellite deduced cloud heights. *J. Appl. Meteor.*, **17**, 1796-1802.

Stowe, L. L., G. G. Wellemeyer, T. F. Eck, H. Y. M. Yeh, and the Nimbus-7 Cloud Data Processing Team, 1988: Nimbus-7 global cloud climatology. Part I: Algorithms and validation. *J. Climate*, **1**, 445-470.

Stowe, L. L., R. M. Carey, and P. Pellegrino, 1992: Monitoring the Mt. Pinatubo aerosol layer with NOAA/11 AVHRR data. *Geo. Res. Letters*, **19**, 159-162

Susskind, J., D. Reuter, and M. T. Chahine, 1987: Cloud fields retrieved from analysis of HIRS/MSU sounding data. *J. Geophys. Res.*, **92**, 4035-4050.

Warren, S. G., C. J. Hahn, J. London, R. M. Chervin, and R. L. Jenne, 1988: Global distribution of total cloud over and cloud type amounts over the ocean. NCAR/TN-317+STR [Available from the National Center for Atmospheric Research, Boulder, CO, 80307]

Weare, B. C., 1992: Variations in Nimbus-7 cloud estimates. Part I: zonal averages., *J. Climate*, 5, 1496-1505.

Wielicki, B. A., and J. A. Coakley, 1981: Cloud retrieval using infrared sounder data: error analysis. *J. Appl. Meteor.*, 20, 157-169.

Wielicki, B. A., and Parker, 1992: On the determination of cloud cover from satellite sensors: the effect of sensor spatial resolution. *J. Geophys. Res.*, 97, 12799-12823.

Wu, M. L. and J. Susskind, 1990: Outgoing longwave radiation computed from HIRS2/MSU soundings. *J. Geophys. Res.*, 95D, 7579-7602.

Wylie, D. P., and W. P. Menzel, 1989: Two years of cloud cover statistics using VAS. *J. Clim. Appl. Meteor.*, 2, 380-392.

Wylie, D. P. and W. P. Menzel, 1991: Two years of global cirrus cloud statistics using HIRS. Technical Proceedings of the Sixth International TOVS Study Conference held 1-6 May 1991 in Airlie, VA, 344-353.

Table 1: HIRS four year global cloud statistics (June 1989 to May 1993) of the frequency of cloud observations for different heights and effective emissivities ($N\epsilon$). $N\epsilon < 0.25$ corresponds to infrared optical depth $\tau < 0.3$; $N\epsilon < 0.5$, $\tau < 0.7$; $N\epsilon < 0.75$, $\tau < 1.4$; and $N\epsilon < 0.95$, $\tau < 3.0$. Percentages are of the total number of observations, clear and cloudy combined. Clouds were not detected in 23.4% of the observations.

	ALL CLOUDS	EFFECTIVE EMISSIVITY				
LEVEL		<0.25	<0.50	<0.75	<0.95	>0.95
<200 hPa	3.5%	1.2%	0.4%	0.3%	0.7%	0.9%
<300 hPa	9.6	2.3	1.9	1.6	2.1	1.7
<400 hPa	10.8	2.5	2.3	2.2	2.4	1.4
<500 hPa	11.0	2.3	2.5	2.6	2.5	1.1
<600 hPa	8.2	1.4	2.2	2.5	0.7	1.4
<700 hPa	7.8	0.6	1.2	1.7	0.7	3.6
<800 hPa	7.6	0.2	0.4	0.4	0	6.6
<900 hPa	11.5	0	0	0	0	11.5
<1000 hPa	6.8	0	0	0	0	6.8
Total	76.8	10.5	10.9	11.3	9.1	35.0

Table 2a: The HIRS global cloud cover from all four years (June 1989 - May 1993). $N\epsilon$ refers to effective emissivity and τ refers to the corresponding infrared optical depth. Numbers are frequency of cloud cover; over 15,000,000 observations are included.

		EFFECTIVE EMISSIVITY (IR OPTICAL DEPTH)		
	None	Thin	Thick	Opaque
		$N\epsilon<0.50$	$0.5<N\epsilon<0.95$	$N\epsilon>0.95$
		$\tau<0.7$	$0.7<\tau<3.0$	$\tau>3.0$
LEVEL				
hi < 400 hPa		11	9	4
mid <700 hPa		10	11	6
low <1000 hPa		1	0	25
Total	23 (clear)	42 (cirrus)		35 (opaque)

Table 2b: The HIRS global cloud cover in the boreal summer from all four years (June 1989 - May 1993). $N\epsilon$ refers to effective emissivity and τ refers to the corresponding infrared optical depth. Numbers are frequency of cloud cover; over 3,300,000 observations are included.

		EFFECTIVE EMISSIVITY (IR OPTICAL DEPTH)		
	No	Thin	Thick	Opaque
		$N\epsilon<0.50$	$0.5<N\epsilon<0.95$	$N\epsilon>0.95$
		$\tau<0.7$	$0.7<\tau<3.0$	$\tau>3.0$
LEVEL				
hi < 400 hPa		11	9	4
mid <700 hPa		10	10	5
low <1000 hPa		0	0	26
Total	25	40		35
	(clear)	(cirrus)		(opaque)

Table 2c: The HIRS global cloud cover in the boreal winter from all four years (June 1989 - May 1993). $N\epsilon$ refers to effective emissivity and τ refers to the corresponding infrared optical depth. Numbers are frequency of cloud cover; over 3,600,000 observations are included.

		EFFECTIVE EMISSIVITY (IR OPTICAL DEPTH)		
	No	Thin	Thick	Opaque
		$N\epsilon<0.50$	$0.5<N\epsilon<0.95$	$N\epsilon>0.95$
		$\tau<0.7$	$0.7<\tau<3.0$	$\tau>3.0$
LEVEL				
hi < 400 hPa		11	10	4
mid <700 hPa		10	11	7
low <1000 hPa		0	0	24
Total	23 (clear)	42 (cirrus)		35 (opaque)

Table 3a: The change in HIRS global cloud cover from year 1 (June 1989 - May 1990) to year 2 (June 1990 - May 1991). $N\epsilon$ refers to effective emissivity and τ refers to the corresponding infrared optical depth. Numbers are frequency of cloud cover in summer and winter of year 2 minus the same in year 1; negative numbers indicate a decrease in cloudiness while positive numbers indicate an increase.

	EFFECTIVE EMISSIVITY (IR OPTICAL DEPTH)		
	Thin	Thick	Opaque
	$N\epsilon<0.50$	$0.5<N\epsilon<0.95$	$N\epsilon>0.95$
	$\tau<0.7$	$0.7<\tau<3.0$	$\tau>3.0$
LEVEL			
hi < 400 hPa	0	1	-1
mid <700 hPa	0	-1	0
low <1000 hPa	0	0	0
Total	0	0	-1

Table 3b: The change in HIRS global cloud cover from year 2 (June 1990 - May 1991) to year 3 (June 1991 - May 1992). Numbers are frequency of cloud cover in summer and winter of year 3 minus the same in year 2.

	EFFECTIVE EMISSIVITY (IR OPTICAL DEPTH)		
	Thin	Thick	Opaque
	$N\epsilon<0.50$	$0.5<N\epsilon<0.95$	$N\epsilon>0.95$
	$\tau<0.7$	$0.7<\tau<3.0$	$\tau>3.0$
LEVEL			
hi < 400 hPa	4	1	0
mid <700 hPa	2	1	-2
low <1000 hPa	0	0	-5
Total	6	2	-7

Table 3c: The change in HIRS global cloud cover from year 3 (June 1991 - May 1992) to year 4 (June 1992 - May 1993). Numbers are frequency of cloud cover in summer and winter of year 4 minus the same in year 3.

	EFFECTIVE EMISSIVITY (IR OPTICAL DEPTH)		
	Thin	Thick	Opaque
	$N\epsilon<0.50$	$0.5<N\epsilon<0.95$	$N\epsilon>0.95$
	$\tau<0.7$	$0.7<\tau<3.0$	$\tau>3.0$
LEVEL			
hi < 400 hPa	0	0	0
mid <700 hPa	2	-1	0
low <1000 hPa	0	0	2
Total	2	-1	2

Table 4a: The HIRS cloud cover in the boreal summer from all four years (June 1989 - May 1993) over North America (29 to 49 N, 70 to 130 W). $N\epsilon$ refers to effective emissivity and τ refers to the corresponding infrared optical depth. Numbers are frequency of cloud cover; over 600,000 observations are included.

		EFFECTIVE EMISSIVITY (IR OPTICAL DEPTH)		
	None	Thin	Thick	Opaque
		$N\epsilon<0.50$	$0.5<N\epsilon<0.95$	$N\epsilon>0.95$
		$\tau<0.7$	$0.7<\tau<3.0$	$\tau>3.0$
LEVEL				
hi < 400 hPa		9	9	6
mid <700 hPa		9	8	8
low <1000 hPa	30	0	0	21
Total	30	35		35
	(clear)	(cirrus)		(opaque)

Table 4b: The VAS cloud cover in the boreal summer from all four years (June 1989 - May 1993) over North America (29 to 49 N, 70 to 130 W). $N\epsilon$ refers to effective emissivity and τ refers to the corresponding infrared optical depth. Numbers are frequency of cloud cover; over 2,200,000 observations are included.

		EFFECTIVE EMISSIVITY (IR OPTICAL DEPTH)		
	None	Thin	Thick	Opaque
		$N\epsilon<0.50$	$0.5<N\epsilon<0.95$	$N\epsilon>0.95$
		$\tau<0.7$	$0.7<\tau<3.0$	$\tau>3.0$
LEVEL				
hi < 400 hPa		10	12	3
mid <700 hPa		2	3	10
low <1000 hPa	27	0	0	33
Total	27	27		46
	(clear)	(cirrus)		(opaque)

Table 4c: The HIRS cloud cover in the boreal winter from all four years (June 1989 - May 1993) over North America (29 to 49 N, 70 to 130 W). $N\epsilon$ refers to effective emissivity and τ refers to the corresponding infrared optical depth. Numbers are frequency of cloud cover; over 600,000 observations are included.

		EFFECTIVE EMISSIVITY (IR OPTICAL DEPTH)		
	None	Thin	Thick	Opaque
		$N\epsilon<0.50$	$0.5<N\epsilon<0.95$	$N\epsilon>0.95$
		$\tau<0.7$	$0.7<\tau<3.0$	$\tau>3.0$
LEVEL				
hi < 400 hPa		9	12	5
mid <700 hPa		9	15	12
low <1000 hPa	24	0	0	14
Total	24	45		31
	(clear)	(cirrus)		(opaque)

Table 4d: The VAS cloud cover in the boreal winter from all four years (June 1989 - May 1993) over North America (29 to 49 N, 70 to 130 W). $N\epsilon$ refers to effective emissivity and τ refers to the corresponding infrared optical depth. Numbers are frequency of cloud cover; over 2,600,000 observations are included.

		EFFECTIVE EMISSIVITY (IR OPTICAL DEPTH)		
	None	Thin	Thick	Opaque
		$N\epsilon<0.50$	$0.5<N\epsilon<0.95$	$N\epsilon>0.95$
		$\tau<0.7$	$0.7<\tau<3.0$	$\tau>3.0$
LEVEL				
hi < 400 hPa		10	15	4
mid <700 hPa		2	6	20
low <1000 hPa	22	0	0	21
Total	22 (clear)	33 (cirrus)		45 (opaque)

Figure Captions

Figure 1: (a) The geographic frequency of transmissive clouds for the boreal summers (June, July, August) during the observation period June 1989 thru May 1993. The left margin of the figure coincides with the International Date Line.

Figure 1: (b) The geographic frequency of transmissive clouds for the boreal winters (December, January, and February) during the observation period June 1989 thru May 1993.

Figure 2: The frequency of high clouds (cloud pressure < 500 hPa) over ocean is shown in the upper panel as a function of latitude for the boreal summers (June, July, August) of 1989-92 and winters (December, January, February) 1989-93, expressed as a fraction of all satellite observations, clear and cloudy combined. The same over land is shown in the lower panel.

Figure 3: The frequency of thin transmissive clouds ($N\epsilon < 0.5$, $\tau < 0.7$) over ocean is shown in the upper panel as a function of latitude as a fraction of all satellite observations, clear and cloudy combined. Land is shown in the lower panel.

Figure 4: (a) The geographical distribution of the difference in the probability of cirrus in the four boreal summers, 1990 minus 1989 upper left panel, 1991 minus 1990 upper right and 1992 minus 1991 in the lower left. The boreal summer includes the months of June, July, and August.

Figure 4: (b) The geographical distribution of the difference in the probability of cirrus occurring in the four boreal winters. Winter 1990-91

minus winter 1989-90 is the upper left panel, winter 1991-92 minus 1990-91 is the upper right panel and winter 1992-93 minus 1991-92 is the lower left panel. Boreal winter includes the months of December, January, and February.

Figure 5: Monthly time series of high cloud (over 500 hPa) observations from 65 S to 65 N latitude (solid line), light cirrus with $N\epsilon < 0.5$, $\tau < 0.7$ in the tropics from 20 S to 20 N (triple dash), all high clouds (over 500 hPa) in the tropics, 20 S to 20 N (dash), and light cirrus ($N\epsilon < 0.5$, $\tau < 0.7$) in the eastern Pacific Ocean from 10 S to 10 N, 110 W to 170 W (dash dot).

Figure 6: The diurnal change from the seasonal mean of all cloud observations expressed as a change in percentage points of the total clear and cloudy observations. Midnight represents the NOAA 11 evening pass which actually occurred between 0100 and 0300 a.m. local time. Sunrise is the morning NOAA 10 or 12 pass nominally from 0700 to 0800 a.m. local time. Local Noon is the afternoon NOAA 11 pass from 0100 to 0300 p.m. Sunset is the evening NOAA 10 or 12 pass from 0700 to 0800 p.m.

Figure 7: Same as Figure 6 for the change in the frequency of high cloud observations (pressure less than 500 hPa).

Figure 8: Plot of AVHRR cloud fraction N_A (determined from infrared brightness temperature comparison to surface temperature within a collocated HIRS FOV) versus the HIRS CO_2 slicing effective emissivity $N\epsilon_H$ for 6 and 12 January 1994 over the Atlantic Ocean.

Figure 9: AVHRR infrared window image from 6 January 1994 over the Atlantic Ocean from which the cloud fraction versus effective emissivity study was made. HIRS CO_2 cloud pressures are indicated in hPa divided by ten.

Figure 10: The frequency of high cloud observations (cirrus and opaque above 500 hPa) reported by VAS and HIRS during four years (June 1989 to May 1993) in the boreal winter months (December, January, and February) and in the boreal summer months (June, July, and August). Grey shades indicate changes of 20%.

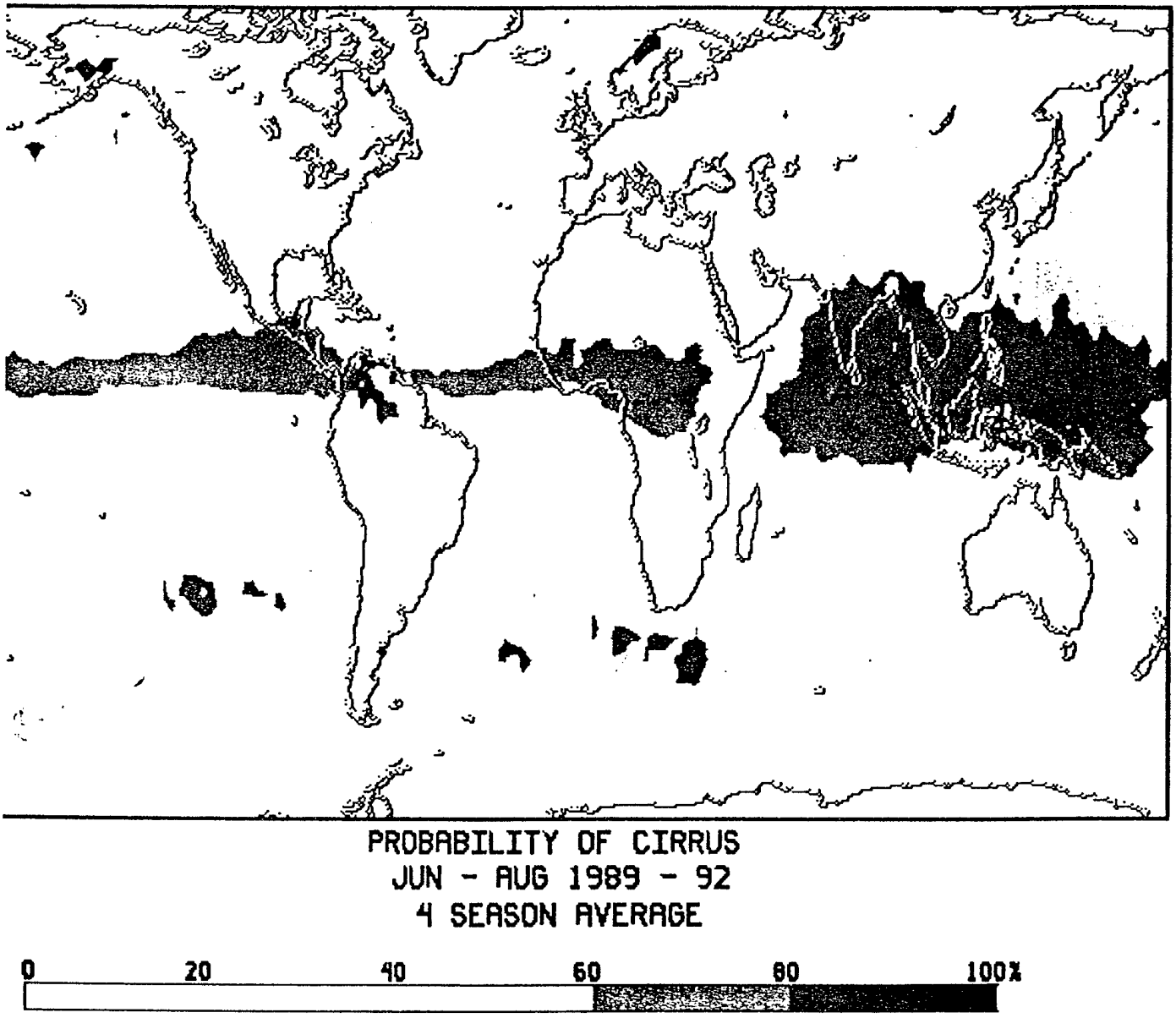

Figure 1: (a) The geographic frequency of transmissive clouds for the boreal summers (June, July, August) during the observation period June 1989 thru May 1993. The left margin of the figure coincides with the International Date Line.

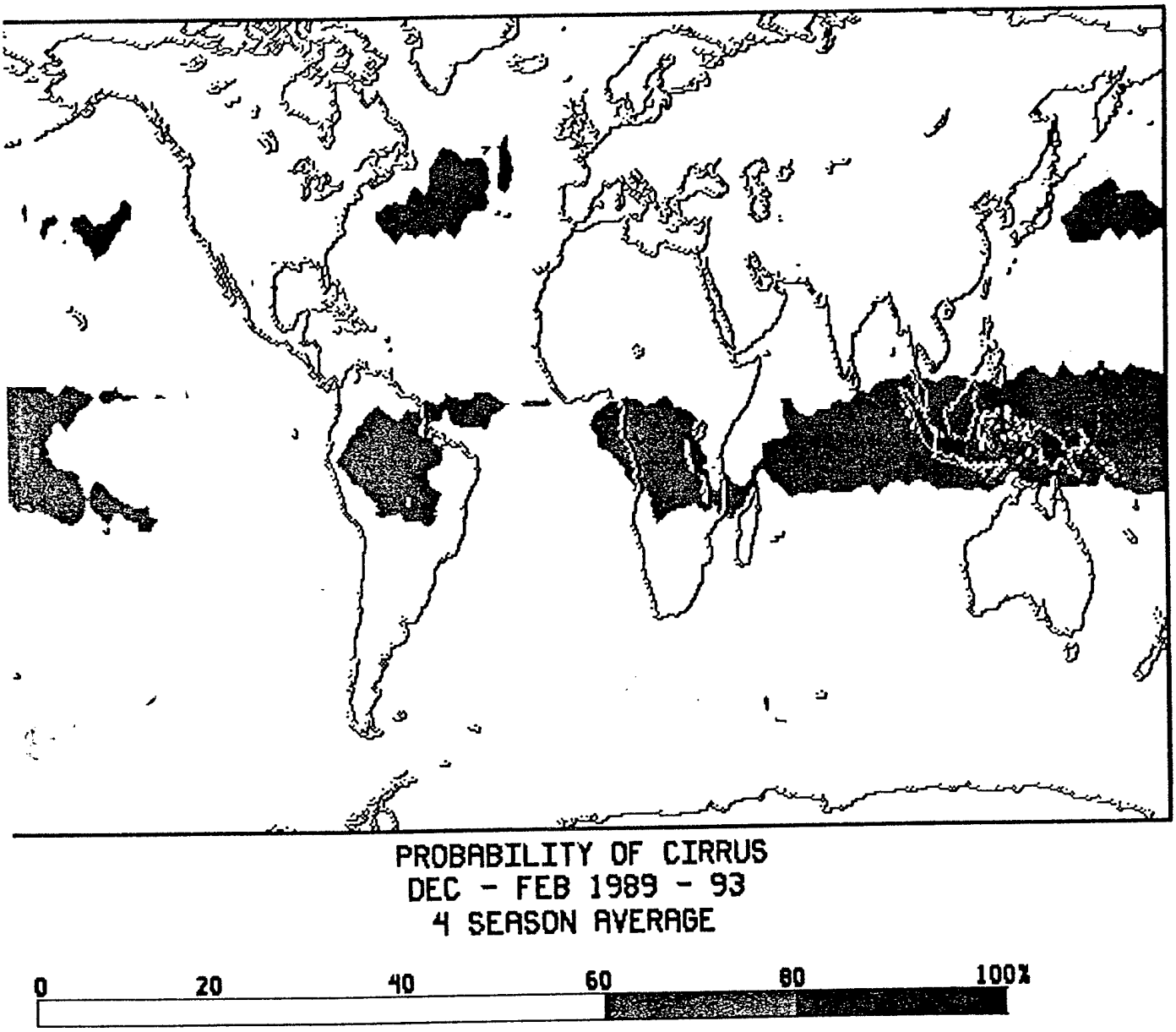

Figure 1: (b) The geographic frequency of transmissive clouds for the boreal winters (December, January, and February) during the observation period June 1989 thru May 1993.

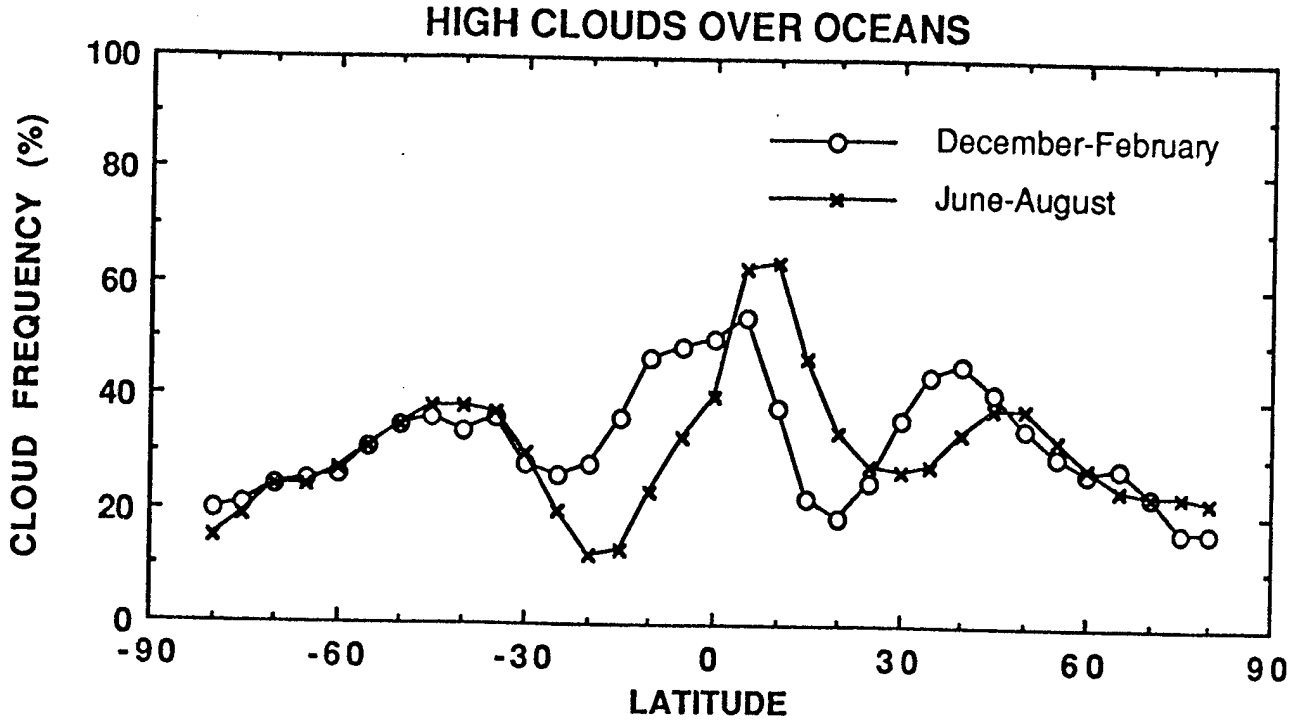

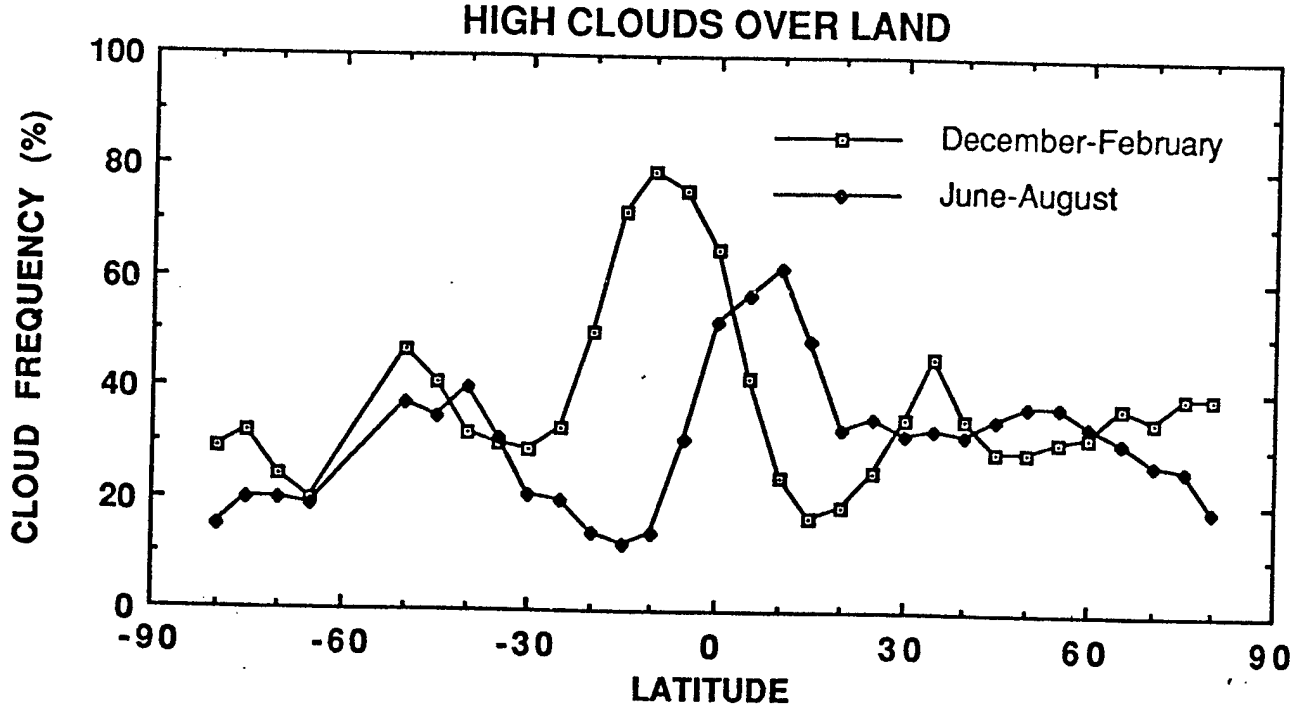

Figure 2: The frequency of high clouds (cloud pressure < 500 hPa) over ocean is shown in the upper panel as a function of latitude for the boreal summers (June, July, August) of 1989-92 and winters (December, January, February) 1989-93 expressed as a fraction of all satellite observations, clear and cloudy combined. The same over land is shown in the lower panel.

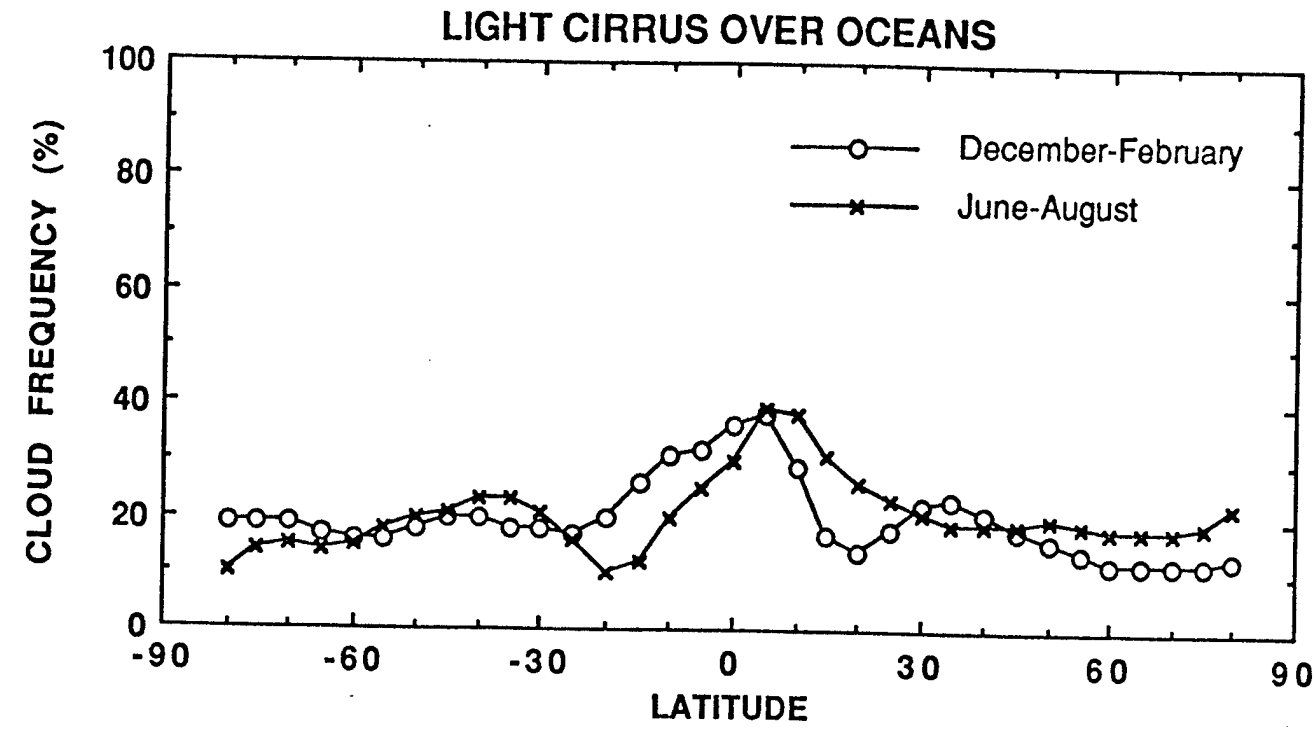

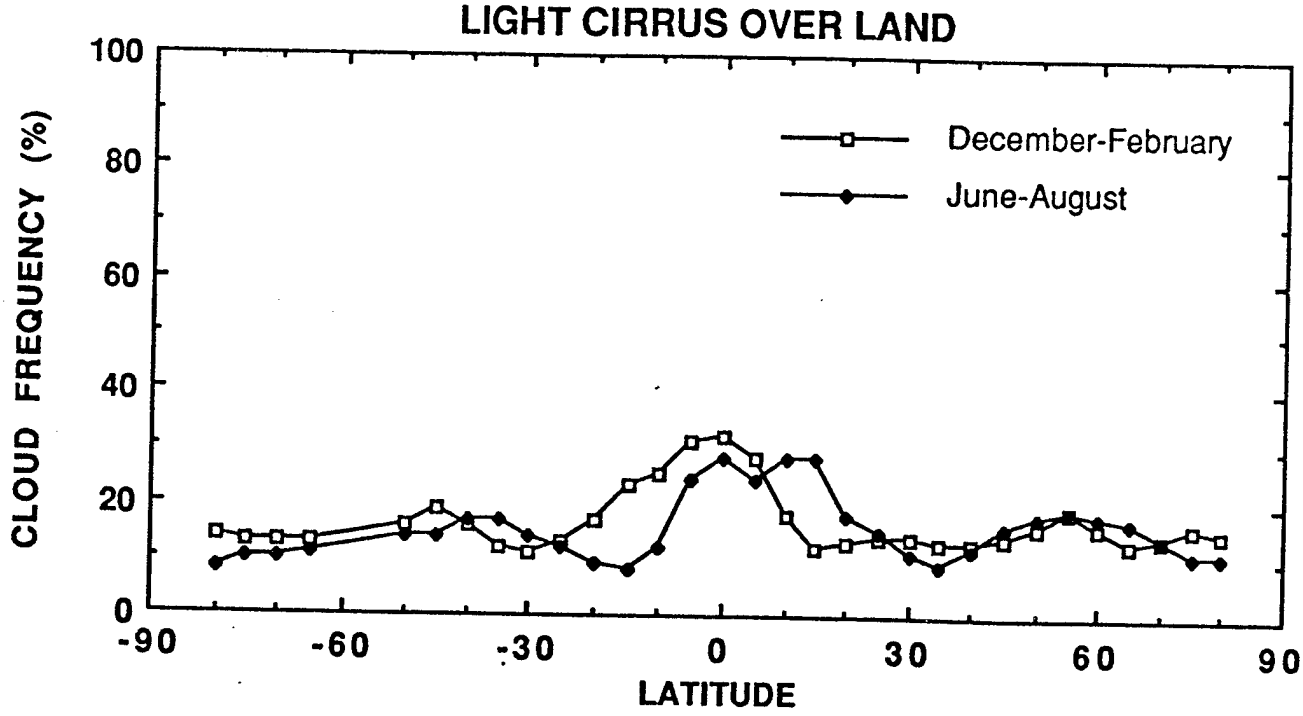

Figure 3: The frequency of thin transmissive clouds ($N\epsilon < 0.5$, $\tau < 0.7$) over ocean is shown in the upper panel as a function of latitude as a fraction of all satellite observations, clear and cloudy combined. Land is shown in the lower panel.

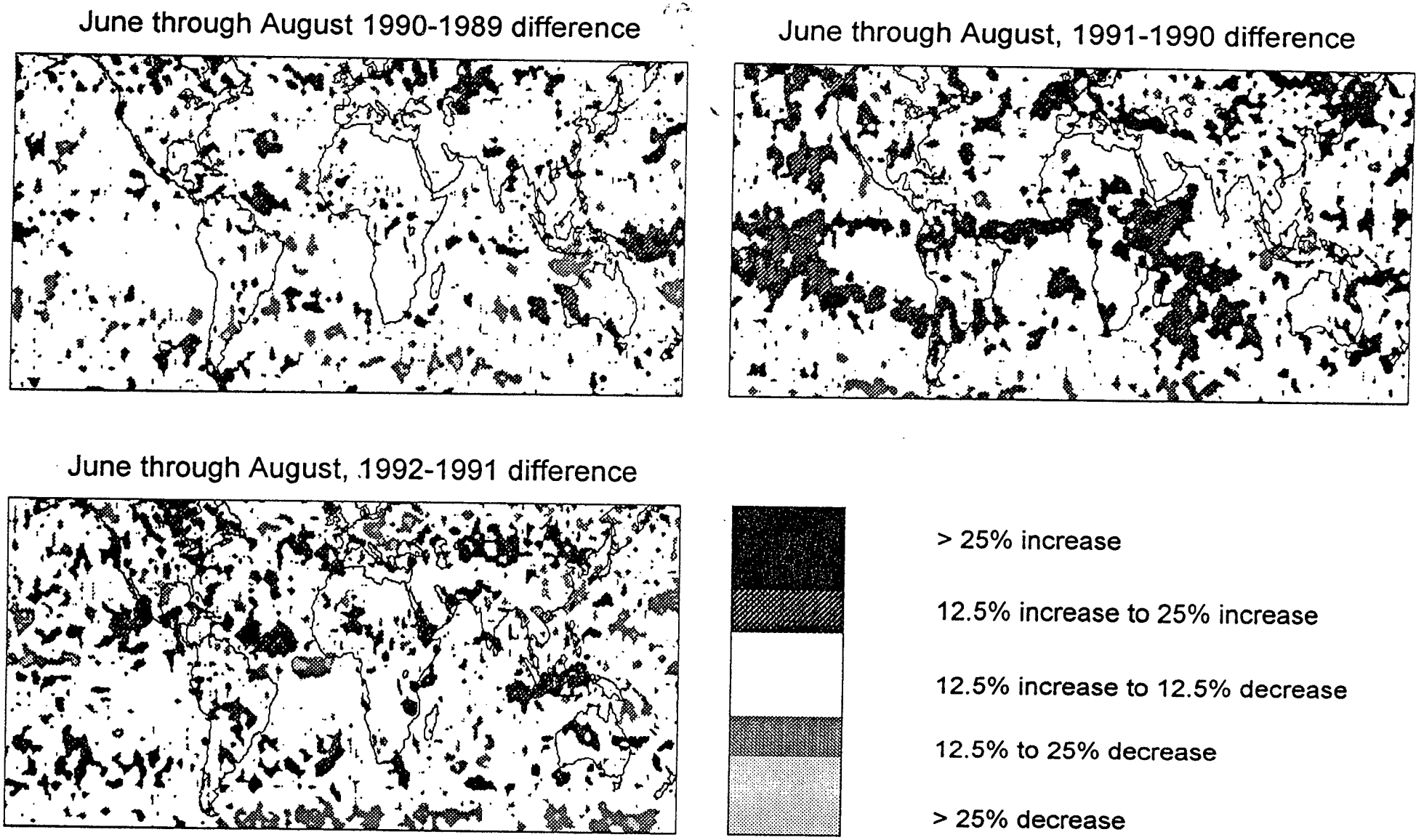

Figure 4: (a) The geographical distribution of the difference in the probability of cirrus in the four boreal summers, 1990 minus 1989 upper left panel, 1991 minus 1990 upper right and 1992 minus 1991 in the lower left. The boreal summer includes the months of June, July, and August.

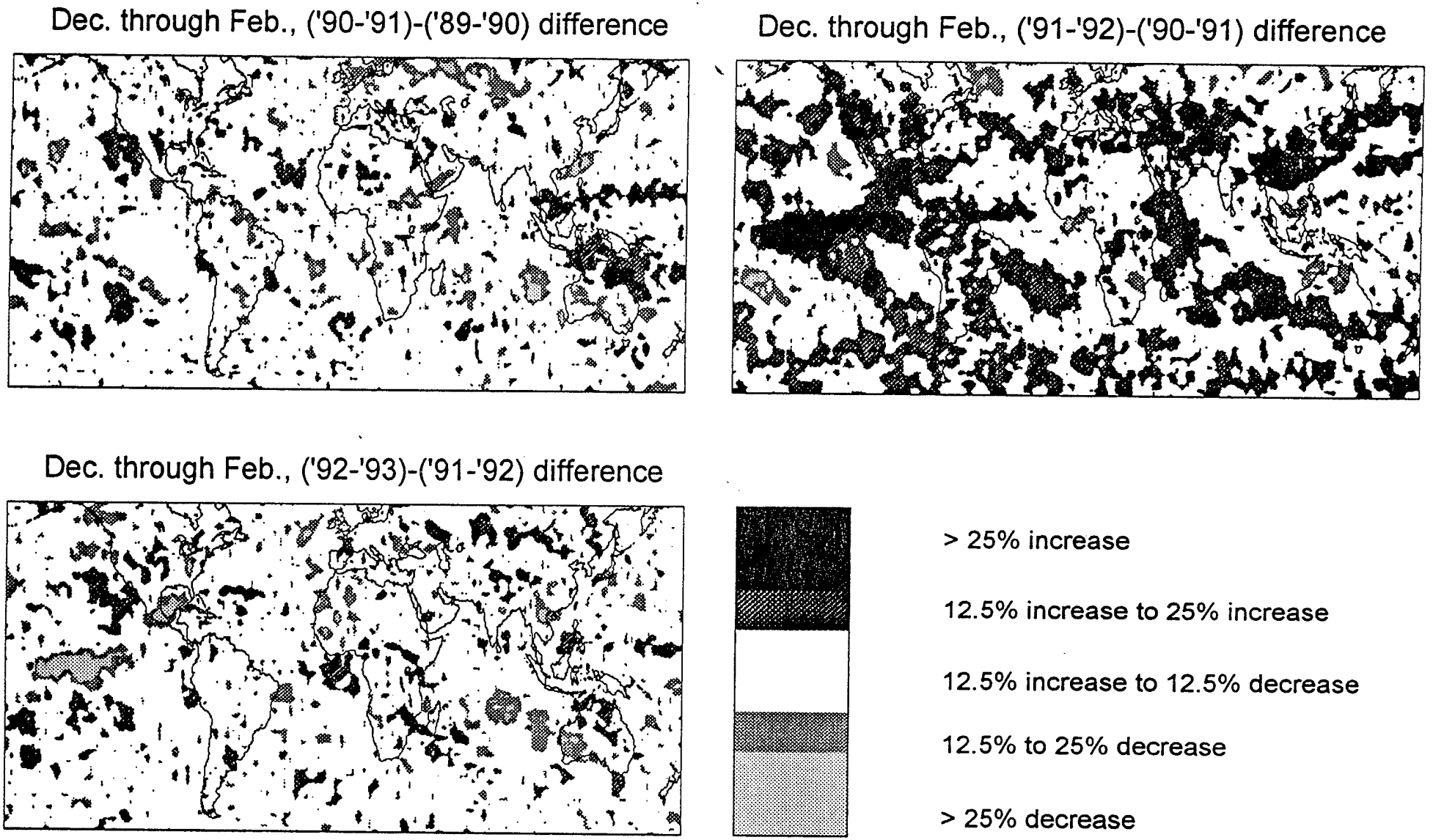

Figure 4: (b) The geographical distribution of the difference in the probability of cirrus occurring in the four boreal winters. Winter 1990-91 minus winter 1989-90 is the upper left panel, winter 1991-92 minus 1990-91 is the upper right panel and winter 1992-93 minus 1991-92 is the lower left panel. Boreal winter includes the months of December, January, and February.

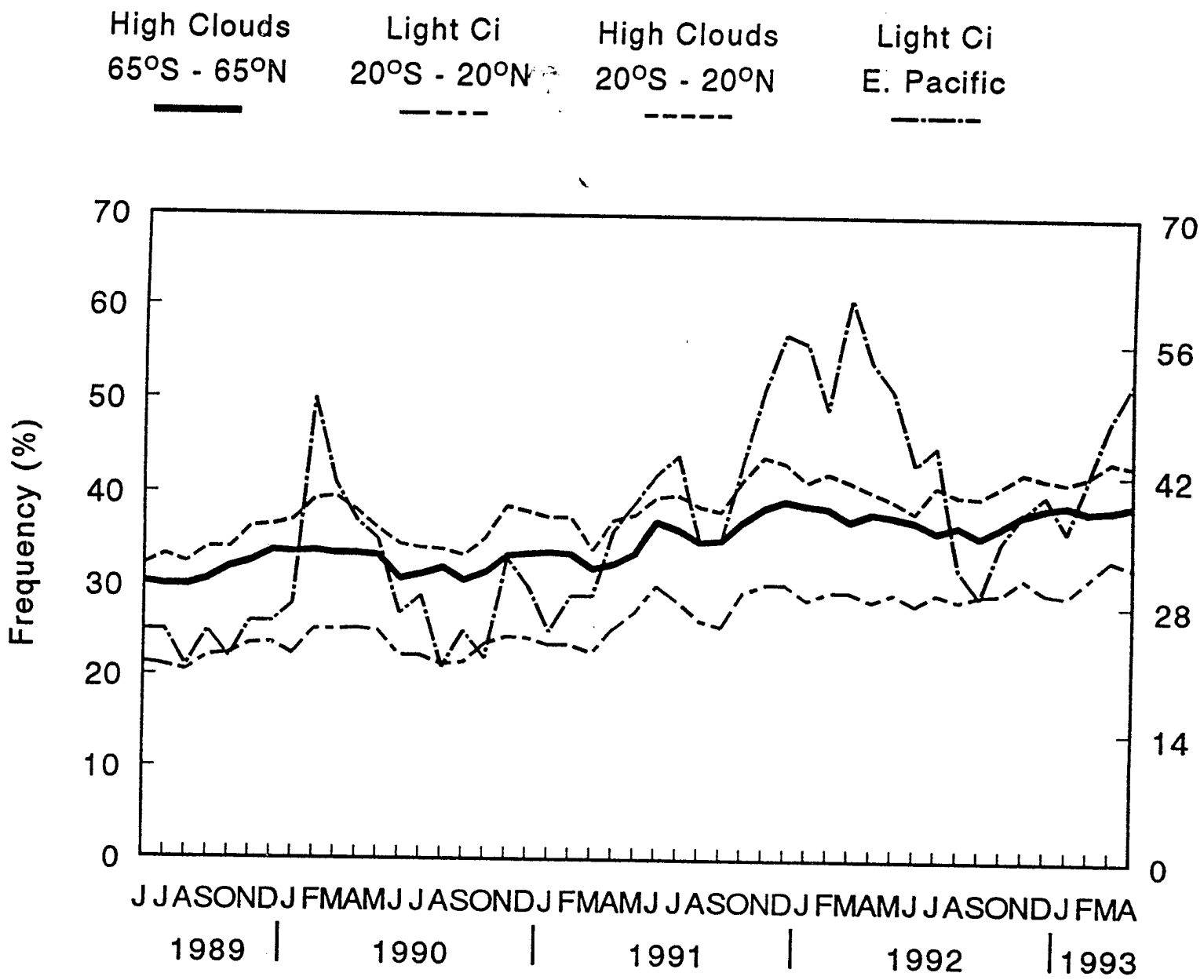

Figure 5: Monthly time series of high cloud (over 500 hPa) observations from 65 S to 65 N latitude (solid line), light cirrus with $N\epsilon < 0.5$, $\tau < 0.7$ in the tropics from 20 S to 20 N (triple dash), all high clouds (over 500 hPa) in the tropics, 20 S to 20 N (dash), and light cirrus ($N\epsilon < 0.5$, $\tau < 0.7$) in the eastern Pacific Ocean from 10 S to 10 N, 110 W to 170 W (dash dot).

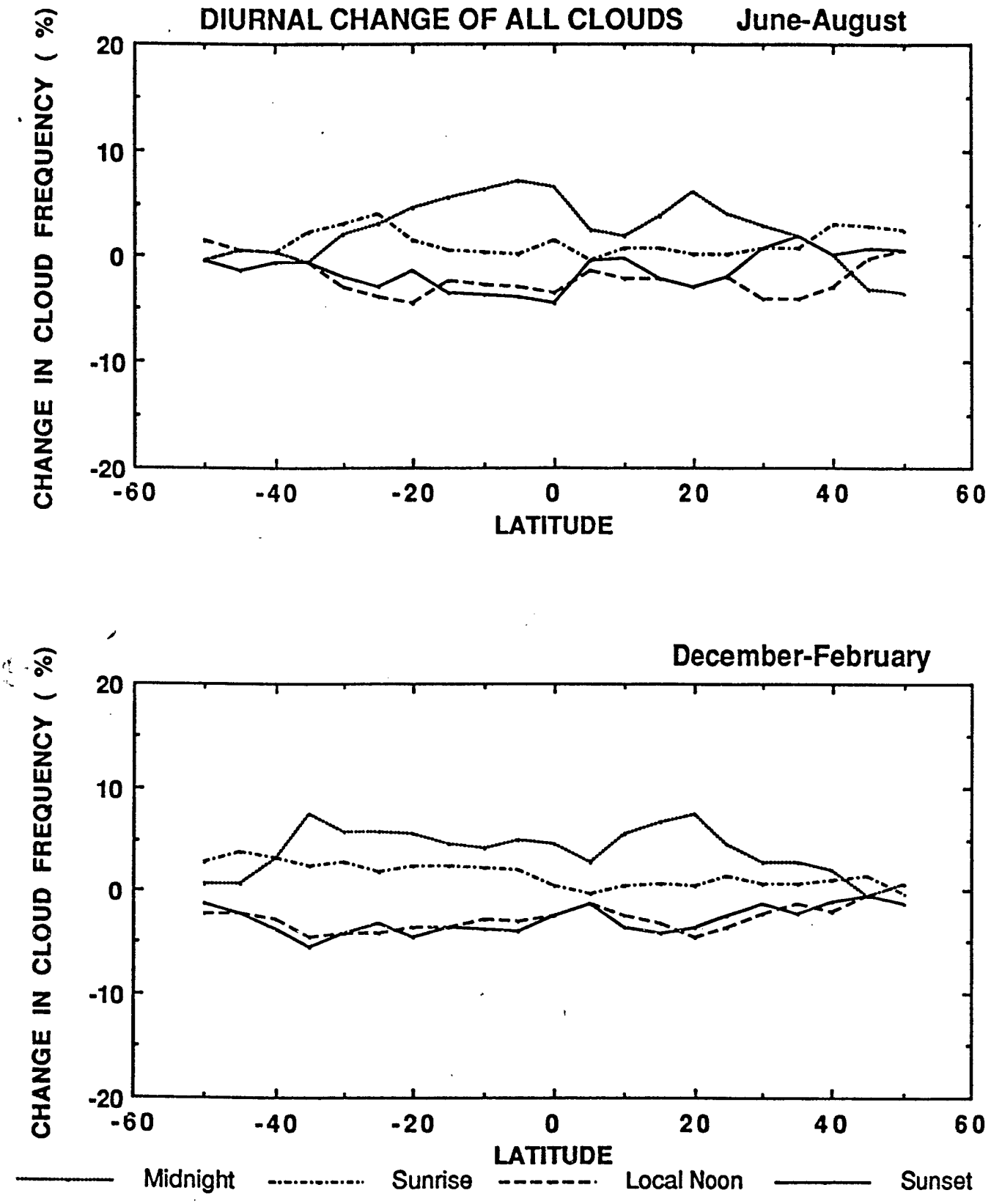

Figure 6: The diurnal change from the seasonal mean of all cloud observations expressed as a change in percentage points of the total clear and cloudy observations. Midnight represents the NOAA 11 evening pass which actually occurred between 0100 and 0300 a.m. local time. Sunrise is the morning NOAA 10 or 12 pass nominally from 0700 to 0800 a.m. local time. Local Noon is the afternoon NOAA 11 pass from 0100 to 0300 p.m. Sunset is the evening NOAA 10 or 12 pass from 0700 to 0800 p.m.

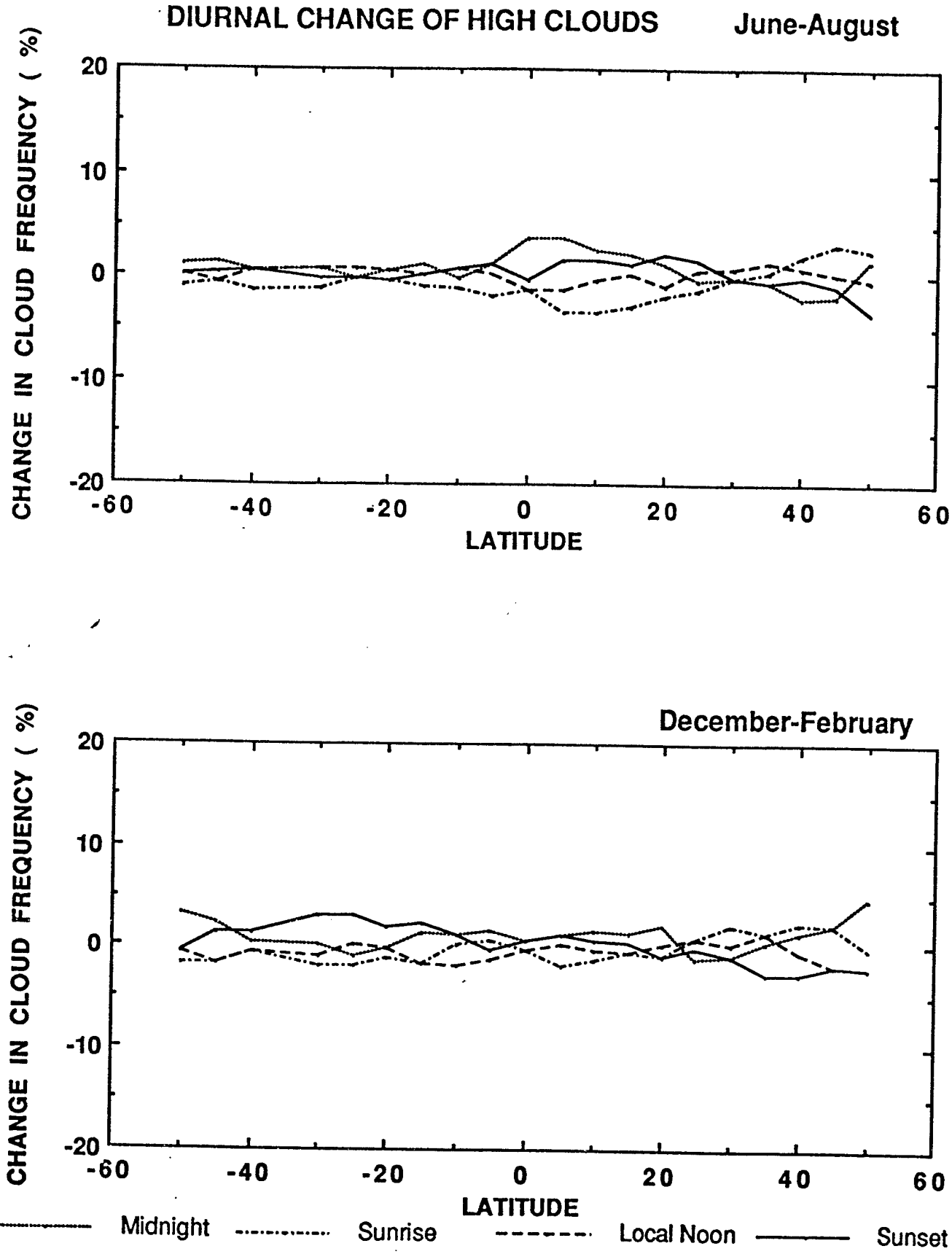

Figure 7: Same as Figure 6 for the change in the frequency of high cloud observations (pressure less than 500 hPa).

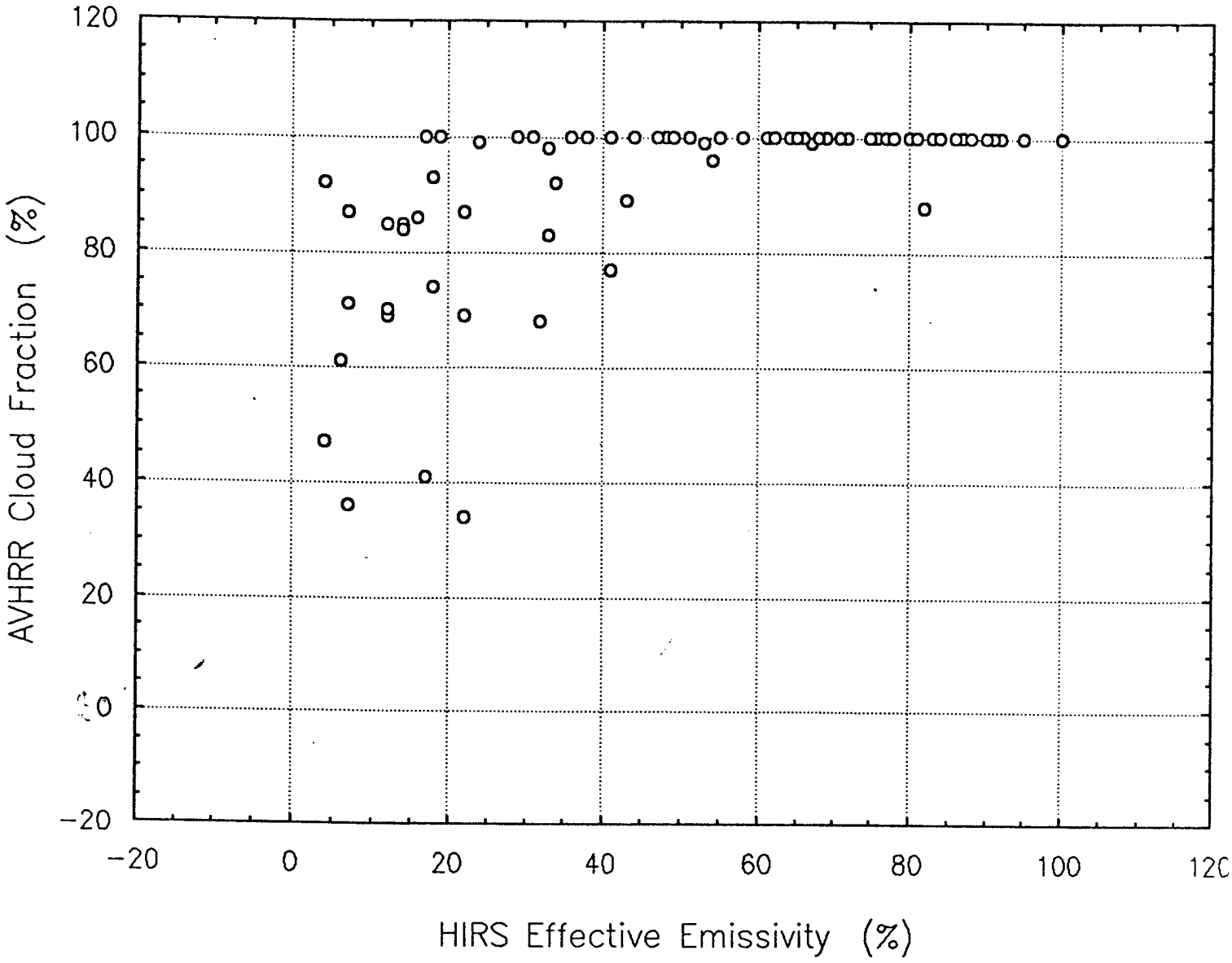

Figure 8: Plot of AVHRR cloud fraction N_A (determined from infrared brightness temperature comparison to surface temperature within a collocated HIRS FOV) versus the HIRS CO_2 slicing effective emissivity $N\epsilon_H$ for 6 and 12 January 1994 over the Atlantic Ocean.

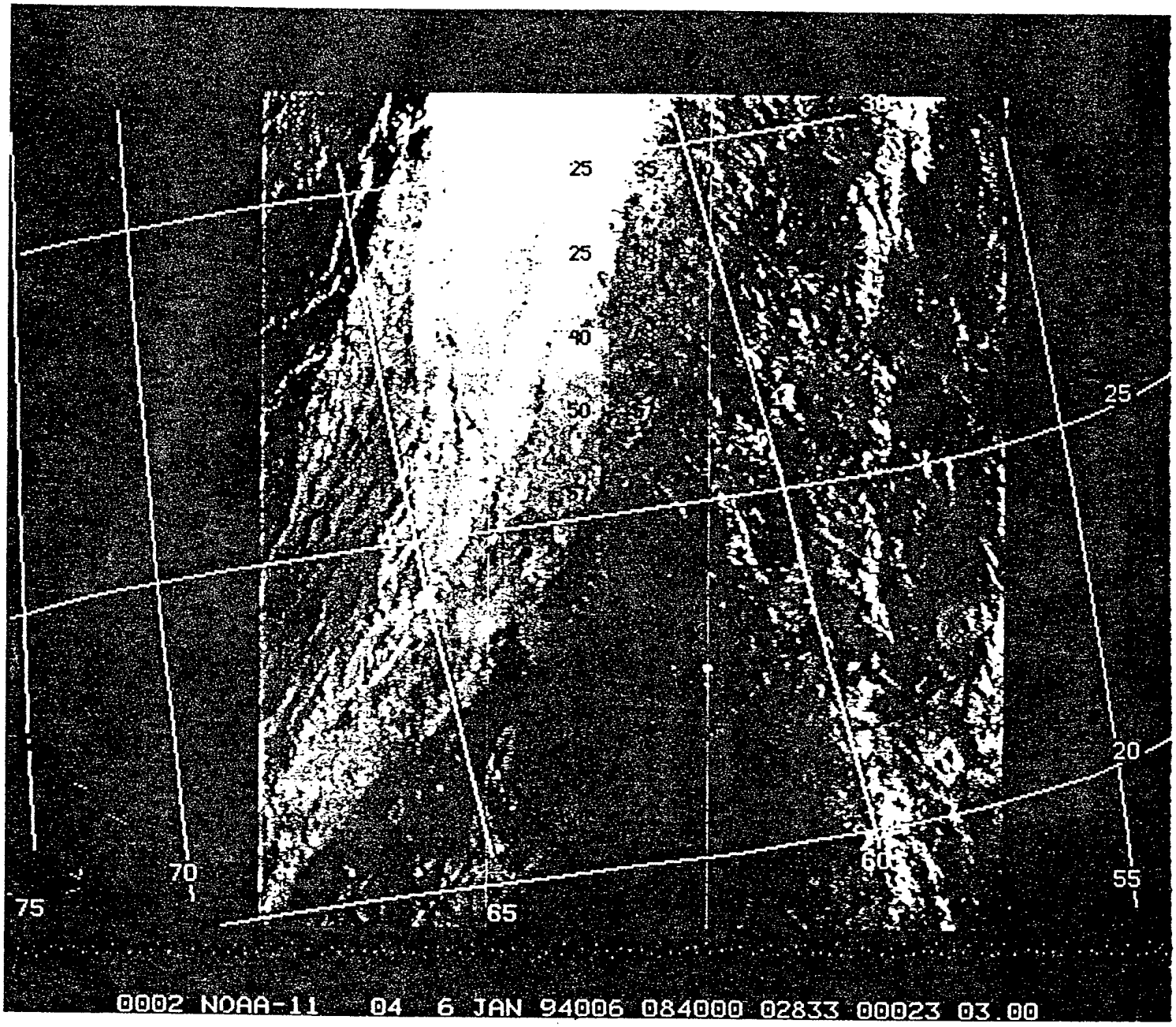

Figure 9: AVHRR infrared window image from 6 January 1994 over the Atlantic Ocean from which the cloud fraction versus effective emissivity study was made. HIRS CO_2 cloud pressures are indicated in hPa divided by ten.

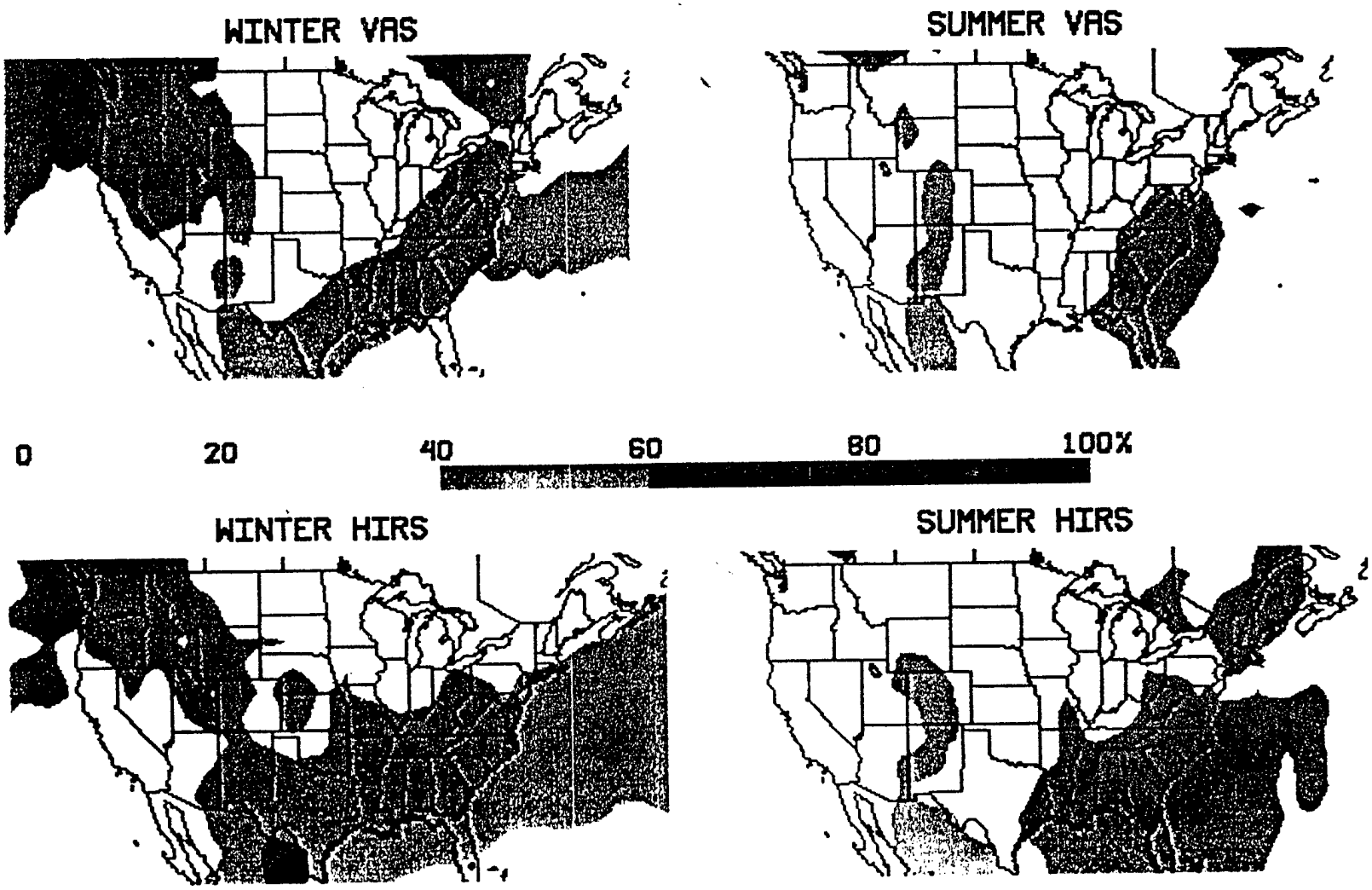

Figure 10: The frequency of high cloud observations (cirrus and opaque above 500 hPa) reported by VAS and HIRS during four years (June 1989 to May 1993) in the boreal winter months (December, January, and February) and in the boreal summer months (June, July, and August). Grey shades indicate changes of 20%.